The Islamic University – Gaza
Higher Education Deanship
Faculty of Engineering
Civil Engineering Department
Design and Rehabilitation
of Structures

الجامعـــــة الإســـــلامية – غـــزة
عمـــــادة الدراســـــات العليـــا
كـــــليـــــة الهنـــدســـــة
قـــــسـم الهنـــدســة المدنيـــة
تصـــــميـم وتـــأهيـل منشـــآت

التحليل اللاخطي بطريقة العناصر المحدودة للجوائز الخرسانية المسلحة والمدعمة بالطبقات الخرسانية المسلحة بالألياف الفولاذية

Nonlinear Finite Element Analysis of RC Beams Strengthened with Steel Fiber-Reinforced Concrete (SFRC) overlays

Submitted By:
Mohammed Hussein Ashour

Advisor:
Dr. Nasreddin Elmezaini

A Thesis Submitted in Partial Fulfillment of Requirements for the Degree of Master of Science in Civil Engineering
Design and Rehabilitation of Structure

DEDICATION

To my father, **Dr. Hussein**, my mother, **Wafa'**

To my wife, **Heba**, who I hold most dear

To my daughter, **Sara**, and my son, **Hussein** … life without you is colorless

To my brothers, **Ibrahim**, **Ahmed**, **Mahmoud** and **Mostafa**, and my sister **Heba**

To my close friend, **Mohammed Syam**, who gave up his life defending our land in 2014 war

To all of you, and for your unbounded support and love … I dedicate this thesis.

ACKNOWLEDGEMENT

First and foremost, I would like to thank my advisor **Dr. Nasreddin Elmezaini**. I deeply appreciate his guidance throughout the thesis preparation. I am thankful to him eternally for his time, suggestions and ideas. His thoughts and insightful remarks made a significant contribution to the thesis.

In addition, I would like to thank my best friend **Hussein AliHussein**, who put the idea of joining the master program at IUG in my head, if it was not for him, I would not be writing those words now.

Moreover, I would like to thank my friend **Ruba Jamal**, who helped me gathering the resources and literature materials.

Many thanks to my family, my friends and my colleagues at work for the help and inspiration.

Abstract

The behavior of RC beams strengthened with steel fiber-reinforced concrete (SFRC) overlays was studied by Finite Element Analysis software ANSYS. Four beams, three of them were experimentally tested in previous research were considered. The first beam was considered as a control beam made of ordinary concrete, while the second one was modeled using SFRC material properties. The third one is a beam with two material properties, the original part, which is made of ordinary concrete that needed to be strengthened and the overlay, which is made of SFRC material. The fourth beam is the same as the third one, except the SFRC, part is at bottom as an underlay. To ensure a monolithical behavior, a weld-bond strengthening techniques were used.

Ordinary concrete, as well, Steel Fiber-Reinforced Concrete was modeled using the multilinear isotropic hardening constants where it is assumed to have a linear behavior up to 30% of compressive strength. Afterwards, a multilinear stress-strain curve was defined. For reinforcing steel, a linear elastic-perfect plastic material model was used. Steel fiber reinforced concrete was modeled using two methods, the smeared model and the discrete model.

The results obtained by FEA showed a good agreement with those obtained by an experimental program. For beams strengthened with SFRC overlays, results indicated a remarkable improvement in the load carrying capacity and ductility by 15% and 8%, respectively. While for beams strengthened with SFRC underlays, results indicated an improvement in both load carrying capacity and overall ductility by about 24% and 162%, respectively. In both cases, the welding of stirrups prevents diagonal cracks from proliferating into the compression zone. A parametric study indicated an improvement in load carrying capacity with higher SFRC compressive strength values, while increasing the fraction volumes in the SFRC overlay did not affect the results significantly.

The results of this research indicated that it is possible to predict the behavior of beams strengthened with SFRC overlays and underlays using FEA without the need for costly experimental testing. While the importance of this research comes from the fact that if the use of numerical analysis can predict the behavior of beams with SFRC overlays, this will help researchers predicting the behavior of beams with different configurations without the need to go through the lengthy experimental programs.

الملخص

تمت دراسة سلوك الجوائز البيتونية المدعمة بطبقات من البيتون المقوى بالألياف المعدنية SFRC باستخدام برنامج العناصر المنتهية ANSYS .

تمت نمذجة أربعة جوائز بيتونية؛ ثلاثة من دراسة سابقة ورابع نظري لم يختبر مسبقاً، من دراسة تجريبية سابقة، الجائز الأول تم اعتباره جائز مقارنة وهو جائز بيتوني عادي غير مدعم، الجائز الثاني هو جائز مكون من البيتون المخلوط بالألياف المعدنية، أما الجائز الثالث فهو مؤلف من جزئين، الأول بيتوني عادي ويمثل الجائز بدون تقوية والجزء الثاني هو طبقة من SFRC تتوضع أعلى الجائز، الجائز الرابع مماثل للجائز الثالث ولكن طبقة SFRC تتوضع أسفل الجائز. جدير بالذكر أن الجائز الرابع لم يختبر مسبقاً. ولضمان عمل الجائز البيتوني مع مادة التقوية بشكل مشترك، تم إجراء عملية لحام معدني في مناطق معينة من الجائز.

تمت نمذجة كلاً من مادتي البيتون العادي والبيتون المقوى بالألياف المعدنية باعتبارهما مادة متماثلة الخواص ذات سلوك متعدد الخطيّة (multilinear)، سلوك مخطط (اجهاد – تشوه) هو سلوك خطي حتى الوصول إلى قيمة 30% من إجهاد الضغط للبيتون، وبعد ذلك يصبح السلوك متعدد الخطية، أما حديد التسليح فقد تمت نمذجته باعتبار سلوكه مرن-تام اللدونة.

النتائج المتحصل عليها من نظرية العناصر المحددة تقارب إلى حد كبير النتائج المخبرية، إذ أنه وللأحزمة الخرسانية المقواة بواسطة طبقات الخرسانة المقواة بالألياف المعدنية المتوضعة أعلى الجائز، تبين أن هناك زيادة بنسبة 15% في مقاومة الجائز، وزيادة بنسبة 8% في مطاوعة الجائز. بينما الأحزمة الخرسانية المقواة بواسطة طبقة من الخرسانة المقواة بالألياف المعدنية المتوضعة أسفل الجائز، فقد أظهرت النتائج يادة في مقاومة الجائز بنسبة 24%، بينما ارتفعت مطاوعة الجائز إلى 162%، وفي كلا الحالتين، فإن إجراء عملية اللحام للأساور قد منعة الشقوق القطرية من الوصول إلى منطقة الضغط في الجائز البيتوني. كما أظهرت دراسة بارامترية تحسنا في مقاومة الجائز مع زيادة قوة الخرسانة، بينما لم تغير نسبة الألياف الفولاذية كثيراً من تصرف الجائز.

تظهر نتائج هذه الدراسة إمكانية تمثيل سلوك الجوائز البيتونية المدعمة بطبقات SFRC سواء المتوضعة أعلى أو أسفل الجائز البيتوني دون الحاجة إلى اللجوء للتجارب المكلفة، وذلك عن طريق التحليل باستعمال نظرية العناصر المنتهية FEM. وتأتي أهمية هذا البحث من إمكانية نمذجة الجوائز البيتونية عددياً باستعمال نظرية العناصر المحددة والتنبؤ بسلوك الجوائز البيتونية المقواة بطبقات SFRC. وبالتالي يمكن التنبؤ بسلوك الجوائز البيتونية المقواة بطرق أخرى دون الحاجة إلى إجراء دراسات تجريبية طويلة.

Contents

List of Tables

List of Figures

Chapter 1
Introduction

The use of steel fiber-added reinforced concrete (SFRC) have become widespread in several structural applications such as tunnel shells, concrete sewer pipes, and slabs of large industrial buildings. Usage of SFRC in load-carrying members of buildings having conventional reinforced concrete (RC) frames is also gaining popularity recently because of its positive contribution to both energy absorption capacity and concrete strength. Recently, SFRC start to make its way into strengthening techniques, such as SFRC overlays for beams, jackets for beams, columns and other structural members. Members fabricated from SFRC exhibited a remarkable improvement in cracks behavior, ductility, compression\tensile strength and durability.

One of the methods to increase load carrying capacity of beams is to add a concrete overlays to the existing beams. The effectiveness of this technique depends on the ability of strengthened beam to act monolithically as one unit while being loaded.

In the last few decade, Finite element theory has been used to study the behavior of reinforced concrete elements subjected to various kinds of loadings, which led to a revolution in the modeling field. FEA would save a lot of time and money, and predict the behavior of structural element with a high level of accuracy. Moreover, FE would be deployed in forensic engineering field, were assessment is required to determine the capacity of the structural elements under consideration.

In this study, the validity of FE numerical analysis will be demonstrated in predicting the behavior of RC beams, which was previously tested in the lab. The beams were strengthened with SFRC overlays, which were mechanically bonded to the original RC beams. The numerical analysis will be carried out using the well-known FE code ANSYS APDL v13.0 multiphysics.

1.1 Problem Statement

Several studies were conducted to investigate the mechanical properties of reinforced concrete beams strengthened with steel fibers under different loading conditions [1, 2, 3, 4, 5, 6]. Many were dedicated to study the behavior of beams made of SFRC [7, 8, 9]. Most of these studies involved experimental tests, yet, to the best knowledge of the author, none was entitled to study the behavior of RC beams strengthened with SFRC overlays numerically.

1.2 Research Aims

The main aim of the research is to predict the behavior and efficiency of RC Beams strengthened with SF overlays numerically, using ANSYS FE code, without the need to go through the lengthy experimental programs.

1.3 Research Objectives

The main objectives of the research are:

1. Demonstrate the capability of ANSYS program in predicting the behavior of RC beams strengthened with SFRC overlays.
2. Calibrate the experimental mechanical properties of SFRC into a FE package.
3. Study the effect of different parameters effect on the behavior of RC beams and SFRC beams, modeled using FE packages, i.e., compressive strength, steel fiber fraction volume and the effect of SFRC overlay versus SFRC underlay.

1.4 Research Importance

The Importance of this research comes from the fact that if the use of numerical analysis can predict the behavior of beams with SFRC overlays, this will help researchers predicting the behavior of beams with different configurations without the need to go through the lengthy experimental programs.

1.5 Research Scope and Limitations

The research will focus mainly on the behavior of beams strengthened with SFRC overlays. The overlay part will be bonded mechanically with the original beam. Full bonding between the overlay and the ordinary concrete is assumed, hence, no contact element will be used.

A proper modeling of such beams requires using suitable numerical parameters regarding material properties, failure surfaces, crack progression and interface interaction, especially when inter-laminar shear failure is expected.

1.6 Research Methodology

Throughout this research, a comprehensive literature review will be carried out at first regarding the mechanical behavior of the reinforced concrete and steel fiber-reinforced concrete, under static monotonic loading.

Then, a detailed review will be carried out about the finite element theory and its structural application in the field of reinforced concrete and SFRC. Recommendations from previous studies will be took into account when coding the FE models of the numerical beams. Results obtained from numerical analysis will be compared to experimental results to validate the aim and objectives of this research. At last, results summarization will be conducted, recommendations will be obtained and conclusions will be stated.

This study involves a numerical analysis of four beams; three of them were experimentally tested in a previous study conducted by Ziara [10]. One beam will be used as a control beam for comparison purposes. The control beam is modeled using conventional ordinary concrete material properties.

Another beam will be modeled using Steel Fiber-Reinforced Concrete (SFRC) material properties. This beam will be compared to the control beam to examine the influence of incorporating the steel fiber material properties into the ordinary concrete material properties.

Another beam will be modeled using two material properties, i.e. ordinary concrete and steel fiber-reinforced concrete. The ordinary concrete section will represent the existing beam, which needs to be strengthened, while the steel fiber-reinforced concrete will represent the strengthening overlay. This beam is set to study the influence of adding an overlay to an existing section of ordinary concrete in terms of load carrying capacity and ductility. The fourth beam will be modeled also with both ordinary concrete and steel fiber-reinforced concrete material properties. In this case, the steel fiber-reinforced concrete section will be used as underlay for comparison purposes with the previous beam.

1.7 Research Structure

The thesis is divided into six chapters. The first chapter summaries the aims, objectives, importance and methodology of the research. The second chapter includes a detailed background and literature review regarding finite element analysis of reinforced concrete, steel fiber reinforced concrete and similar previous works.

The third chapter discuss the numerical modeling of reinforced concrete, steel fiber-reinforced concrete and reinforcing steel. It includes a detailed description about the material constitutive models, failure surfaces and cracks models.

Chapter four is about the finite element modeling of the beams under investigation. This chapter contains a detailed description of the elements been used to model concrete, reinforcing steel and support/loading plates. It also includes a detailed description of the numerical tools that have been used to solve the models.

Chapter five presents the results of the numerical models. A discussion of those results are also included, as well as a section containing a validation of the numerical results against experimental results. Chapter six contains the conclusions of the study and the recommendations.

The chapter will be in the following order:

- Chapter 1: Introduction
- Chapter 2: Background and Literature Review
- Chapter 3: Numerical Modeling of Reinforced Concrete Material
- Chapter 4: Case Study
- Chapter 5: Discussion of FEA Results
- Chapter 6: Summary and Conclusions
- References
- Appendix: *ANSYS APDL FEM code of beam "B1-FEM"*

Chapter 2
Background and Literature Review

2.1 Mechanical behavior of Ordinary Reinforced Concrete

Concrete is a composite material composed of aggregates, chemically bound together by hydrated Portland cement. The aggregate is graded in size from fine sand to gravel with the maximum gravel size in structural concrete commonly being 3/4 in., although 3/8 in. or 3/2 aggregate maybe used [11].

The behavior of reinforced concrete can be roughly divided into three phases: the uncracked elastic stage, crack progression, and the plastic phase. Two major material effects cause the nonlinear response: cracking of concrete and plasticity of reinforcement. Other time-independent nonlinearities arise from the nonlinear action of the individual constituents of reinforced concrete, e.g., bond slip between steel and concrete, aggregate interlock of a cracked concrete and dowel action of reinforcing steel. The time dependent effects such as creep, shrinkage, and temperature change also contribute to the nonlinear response [12].

Three factors must be considered when carrying out a complete progressive-failure of reinforced concrete structures: the loading inputs, the generalized material behavior and the analytical procedures. By loading, we refer to the specific forces and motion that should be considered in the analysis and design of reinforced concrete structures. The generalized material behavior refers to the multidimensional stress-strain relations subjected to monotonic and cyclic loading. These constitutive equations are the most fundamental relations required for any analysis of reinforced concrete structure. While the analytical procedures refers to the mathematical and numerical aspects of calculations used to obtain solutions. In recent years, there has been a growing interest in the application of the finite element procedures to the analysis of reinforced concrete problems [13].

Although concrete is made up of essentially elastic, brittle materials, its stress-strain curve is nonlinear and appears to be somewhat ductile. This can be explained by the gradual development of microcracking within the concrete and the resulting redistribution of stress from element to element in the concrete. When concrete is subjected to compression with a strain gradient, as would

occur in the compression zone of a beam, the effect of the unstable crack progression stage is reduced because, as mortar cracking softens the highly strained concrete, the load is transferred to the stiffer, more stable concrete at points of lower strain nearer the neutral axis. In addition, continued straining and the associated mortar cracking of highly stressed regions is prevented by the stable state of strain in the concrete closer to the neutral axis.

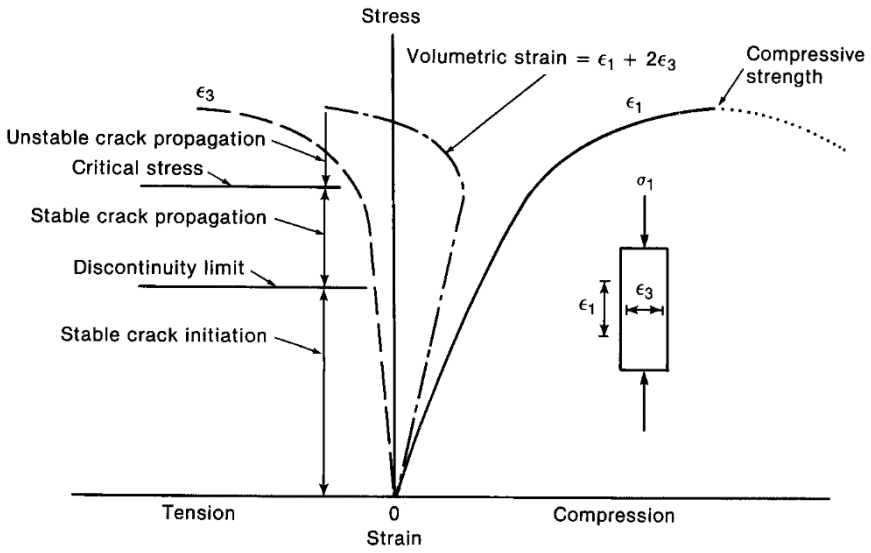

Figure 2-1: Stress-Strain Relationship for Ordinary Concrete *[11]*

As a result, the stable-crack progression stage extends almost up to the ultimate strength of the concrete. Under uniaxial tensile loadings, small-localized cracks are initiated at tensile-strain concentrations and these relieve these strains concentrations. This initial stage of loading results in an essentially linear stress-strain curve during the stage of stable crack initiation. Following a very brief interval of stable crack propagation, unstable crack propagation and fracture occur. The direction of cracking is perpendicular to the principal tensile stress and strain. The tensile strength of concrete falls between 8 and 15 percent of the compressive strength. The actual value is strongly affected by the type of test carried out to determine the tensile strength, the type of aggregate, the compressive strength of concrete and the presence of a compressive stress transverse to the tensile stress [11].

A typical uniaxial stress-strain curve for ordinary concrete is shown in **Figure 2-2**. The maximum stress is reached at strain usually lays between 0.0015 and 0.003, followed by a descending branch. The Shape of this curve results from the gradual formation of microcracks within the structure of

the concrete. The initial slope of the curve (initial tangent modulus of elasticity) increase with compressive strength. This is accounted for by expressing E_c as a function of f_c' [14].

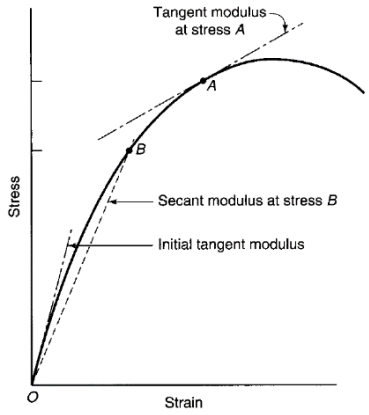

Figure 2-2: Stress-Strain Curve for Ordinary Concrete in Compression *[14]*

For normal-weight concrete with a specific weight "w_c" between 1440 and 2560 kg/m^3, the modulus of elasticity permitted to be taken as $(w_c)^{1.5}\times 0.043\times(f_c')^{1.5}$ [15].

Modified Hognestad stress-strain model is one of the most popular and reliable models used to describe the relationship between stress and strain in concrete. The equations of this model are valid up to a concrete compressive strength of 42 MPa. This model consists of a second-degree parabola with apex at a strain of $1.8\times f_c''/ E_c$, where $f_c'' = 0.9\, f_c'$, followed by a downward-sloping line terminating at a stress of $0.85 f_c''$ and a limiting strain of 0.0038. The stress at any point on the curve in the ascending part is: $f_c'' \left[\frac{2\epsilon_c}{\epsilon_0} - \left(\frac{\epsilon_c}{\epsilon_0}\right)^2\right]$, where $\varepsilon_0 = 1.8\times f_c''/ E_c$, ε_c is the strain at which the stress to be evaluated, and $f_c'' = 0.9\, f_c'$ [16].

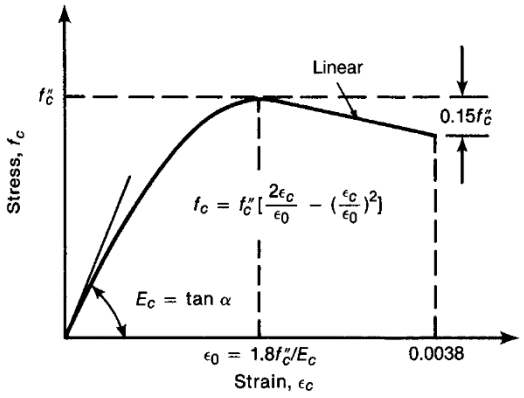

Figure 2-3: Modified Hognestad Model *[16]*

The stress-strain response of concrete loaded in axial tension can be divided into two phases. Prior to the maximum stress, the stress-strain relationship is slightly curved. The stress is linear to roughly 50 percent of the tensile strength. The strain at peak stress is about 0.0001 in pure tension and 0.00014 to 0.0002 in flexural. the rising part of the stress-strain curve be approximated either as a straight line with slope E_c and a maximum stress equal to the tensile strength $f_t^{'}$ or as a parabola with a maximum strain $\varepsilon_t^{'} = 1.8 \times f_t^{'}/E_c$ and a maximum stress $f_t^{'}$. The curve is illustrated in **Figure 2-4** [17].

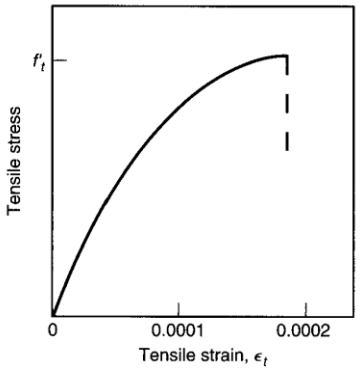

Figure 2-4: Stress-Strain Curve for Concrete in Tension *[17]*

After the Tensile strength is reached, microcracking occurs in a fracture process zone adjacent to the point of the highest tensile stress, and the tensile capacity of this concrete drops very rapidly with increasing elongation. In this stage of behavior, elongations are concentrated in the fracture process zone while the rest of the concrete is unloading elastically. The unloading response is best by a *stress-versus-crack-opening* diagram, idealized in **Figure 2-5** as two straight lines. The crack widths shown in this figure are of the right magnitude, but the actual values depend of the situation. The tensile capacity drops to zero when crack is completely formed. This occurs at a very small crack width [18].

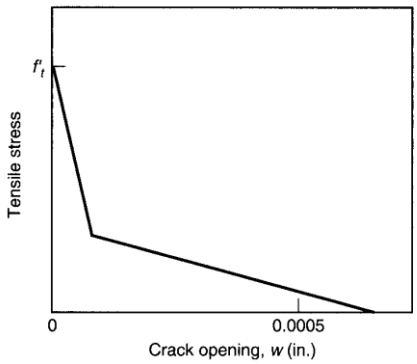

Figure 2-5: Stress-Crack Opening Curve *[18]*

The strength and mode of failure of concrete subjected to biaxial state of stress varies as a function of the combination of the biaxial stress σ_1 and σ_2, which cause cracking or compression failure of the concrete. Under biaxial tension, the strength is close to that in uniaxial tension, where failure occurs by tensile fracture perpendicular to the maximum principle tensile stress. When one principle stress is tensile and the other is compressive, the concrete cracks at lower stress than it would if stressed unaxially in tension or compression. Failure tends to happened due to tensile fractures on planes perpendicular to the principal tensile stresses. The lower strengths in this region suggest that failure is governed by a limiting tensile strain rather than a limiting tensile stress.

Under biaxial compression, the failure pattern changes to a series of parallel fracture surfaces on planes parallel to the unloaded side of the member. Such planes are acted on by the maximum tensile strain. Biaxial and triaxial compression loads delay the formation of the bond cracks and mortar cracks. As a result, the period of stable crack propagation is longer and the concrete is more ductile. As shown in **Figure 2-7**, the strength of the concrete under biaxial compression is greater than the uniaxial compressive strength, which is about 116 % of uniaxial compressive strength. In the web of beams, as shown in **Figure 2-6**, the principle tensile and principal compression stresses lead to a biaxial tension-compression state of stress. Under such loading, the tensile and compressive strengths are less than they would be under uniaxial stress [11].

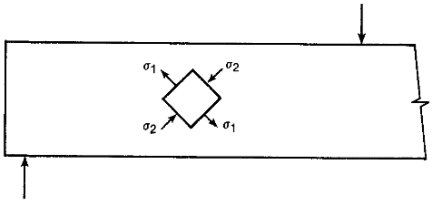

Figure 2-6: Biaxial State of Stress in the Beam Web *[11]*

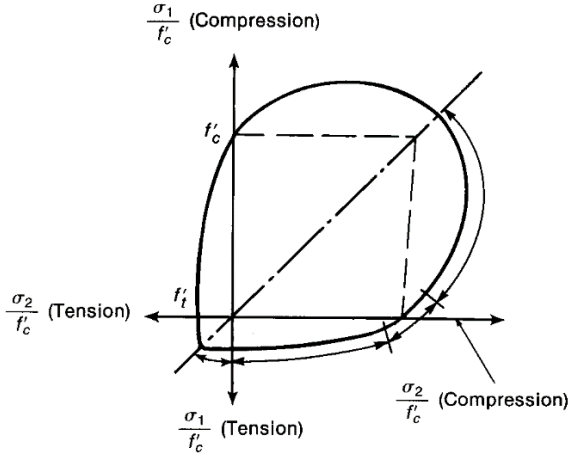

Figure 2-7: Stress at Failure under Biaxial Loading *[11]*

2.2 Behavior of Steel Fiber-Reinforced Concrete

The relationship between steel and concrete has long been regarded as a major stepping-stone in modern construction. Concrete is strong in compression but weak in tension and brittle in nature. To compensate, steel is added to concrete to provide tensile strength. Traditional steel reinforcement is able to distribute the tensile strain forces that cause concrete to crack and ultimately fail. While this system has been successful for many years, there are a number of associated drawbacks. Most serious of all, steel is highly corrosive in nature, which commonly leads to concrete cancer. Concrete cancer refers to the corrosion of reinforcement leading to failure of the structure, which is extremely expensive to repair. The need to enhance concrete tensile behavior with a non-corroded material started in the early 1950's and gave rise to the development of composite materials. By the 1970's steel fiber reinforcement had been accepted as a viable alternative to traditional reinforcement [19].

Addition of steel-fibers to ordinary concrete improves tensile strength significantly among other engineering properties. Flexural strength, fatigue strength and the ability to resist cracking and spalling are also enhanced. Considerable work has been done on the mechanical properties of steel-fiber reinforced concrete. The effect of addition of steel-fibers on compressive strength ranges from negligible to marginal and sometimes up to 25%. Considerable increase in strain at peak stress and the toughness of the material has been observed.

The addition of steel-fibers increased the strain corresponding to the peak stress. The strain capacity and the elastic deformation capability of the concrete matrix in the pre-failure zone are increased considerably with the inclusion of steel-fibers. As shown in **Figure 2-8**, Increase in peak strain, is maximum for fibers having higher volume fraction and for higher aspect ratios. Volume fraction is the weight of steel fibers added to a cubic meter of concrete, while aspect ratio refers to the ratio of *l/d*, where *l* is the length of the fiber and *d* is the diameter. Both ascending and descending portion of the stress-strain curves for steel fiber-reinforced concrete are affected by the addition of steel-fibers. However, the significant effect is noticed in the descending portion of the stress-strain curve. The slope of the descending part of the stress-strain curve, decreases with increase in fiber content at a constant aspect ratio and with increase in aspect ratio for constant volume fraction [20].

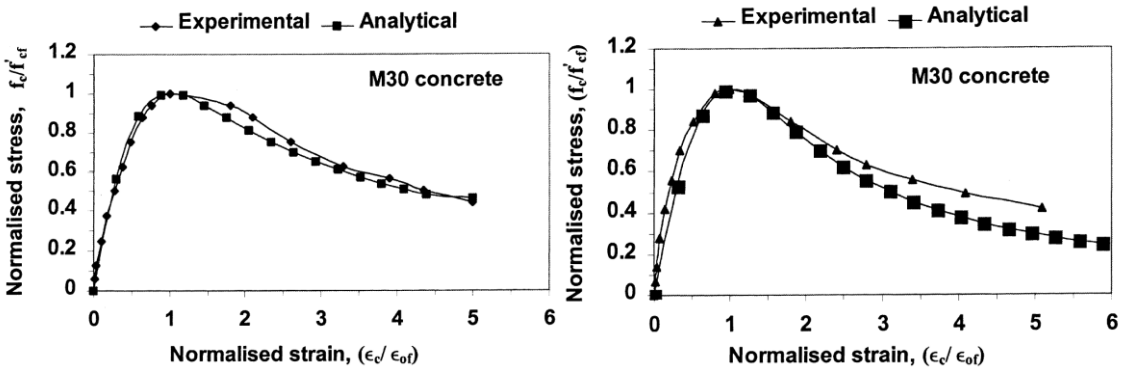

Figure 2-8: Normalized stress-strain curves for steel-fiber reinforced concrete, LEFT: (aspect ratio = 55, volume fraction: 1.0%), RIGHT: (aspect ratio = 55, volume fraction = 0.75%) [20] .

The shear strength and ductility of ordinary concrete is significantly affected by presence of steel fibers, where the load at which the longitudinal reinforcement yields increases. The main effect of the steel fibers is related to the increase of the beam's shear strength, the increase in the load level corresponding to the first shear crack, and therefore, improved shear behavior when compared with a reference beams with stirrups. The shear strength of the fiber reinforced concrete beams with fiber volume of 1.5% is about 30% higher than the nominal design capacity computed by the ACI 318 Code.

Increased fiber volumes allow the development of multiple cracking in beams; smaller crack widths will developed for beams with higher concrete compressive strength due to denser concrete matrix, better bond to the fibers and due to the load transfer across the cracks [21].

Addition of steel fiber would not significantly affect the compressive strength and modulus of elasticity. On the contrary, the split tensile strength were significantly improved so is the toughness of the material. The increase in steel fiber dosage would result in an increase in split tensile strength. The increase in tensile strength ranges from 28% to 35% for SF dosage of 30 kg/m3 and 60 kg/m2, respectively, when being compared to the same grade of ordinary concrete. The tensile strength of SFRC with dosage of 30 kg/m3 and 60 kg/m3 would be roughly lies in between 9% to 12% of compressive strength. Results from previous works indicated a content of 30kg/m3 would be optimum in terms of compressive strength, tensile strength, modulus of elasticity and toughness [22].

Addition of steel fibers to RC beams under monotonic increasing load would result in a smaller crack width. For beams under sustained loading, the increase in crack width was smaller and stabilized at early ages when being to conventional RC beams [23].

The compressive strength of high-strength concrete improved with additions of steel fibers at various volume fractions. The strength showed a maximum at 1.5% fraction but a slight decrease at 2% fraction compared to 1.5%, remaining 12.9% higher than before the fiber addition.

The compressive strength of the fiber-reinforced concrete reached a maximum at 1.5% volume fraction, being a 15.3% improvement over the high-strength concrete. The splitting tensile strength and modulus of rupture of the fiber-reinforced concrete improved with increasing the volume fraction, achieving 98.3% and 126.6% improvements, respectively, at 2.0% volume fraction.

The compressive strength of high-strength concrete improved with additions of steel fibers at various volume fractions. The splitting tensile strength and modulus of rupture of high-strength steel fiber-reinforced concrete both improved with increasing fiber volume fraction. The splitting tensile strength ranged from 19.0% to 98.3% higher for the fractions from 0.5% to 2.0%. In addition, the modulus of rupture ranged from 28.1% to 126.6% higher for the fraction from 0.5% to 2.0% [24].

2.3 Literature Review for SFRC

Steel Fibers draw the attention of many researchers in the last decade, mainly in the strengthening field, due to its ability to enhance strength, ductility and durability of RC members. However, most of the researches were devoted to study the mechanical properties of SFRC, and its influence on flexural, shear and torsional behavior of beams. Following are brief summarization for some of the related publications.

Ding and Kusterle [25] investigated the properties of steel fiber-reinforced concrete/shotcrete at early ages. They found out that addition of steel fibers has improved the mechanical properties of the concrete/shotcrete, where it enhanced the ductility. However, it was found that both strength and ductility could be improved to a certain level when increasing the dosage of the steel fibers. The results obtained by Ding and Kusterle indicated that a steel fiber of 40 kg/m3 would result in the optimum compressive strength. Fibers embedded in the matrix affect the stress and strain

fields, enhancing the stress redistribution and reducing strain localizations. The duration of the peak load for SFRC was much more than plain concrete. Results indicated an enhancement in energy absorption capacity of SFRC.

Nataraja et. al. [20] worked on an experimental investigation to generate a stress-strain curve for steel fibers reinforced concrete for compressive strength ranging from 30 to 50 MPa. Round crimped fibers with three volume fractions of 0.5%m 0.75% and 1.0% and two aspect ratios of 55 and 82 are considered. An analytical model was proposed to generate both the ascending and descending portions of the stress-strain curve. A good correlation between experimental and analytical model was obtain.

Altun et. al. [22] studied the mechanical properties of SFRC. A different dosage of 0 kg/m3, 30 kg/m3 and 60 kg/m3 were used in the study. Nine C20 class RC beams of 300mmx300mmx2000mm dimension and same reinforcement having SF at dosage of 0 kg/m3, 30 kg/m3 and 60 kg/m3 were studied. Another nine of C30 class RC beams with the same dimensions, reinforcement and SF dosage were tested. It was found out that when SF dispersed homogeneously, they act like small bridges, help for better distribution of tensile, and shear stress. Therefore, the cracks are smaller and they are spread more evenly. Results from experiments indicated that only a small improvement in toughness achieved when using 60 kg/m3 SF dosage instead of 30 kg/m3. Which make the 30kg/m3 a better choice. Bending experiments on so many beams indicated that beams with SF dosage of 30 kg/m3 exhibited a remarkable increasing in strength when compared to RC beams without steel fibers.

Mansur and Paramasivam [26] studied the behavior of SFRC beams subjected to pure torsion. The main parameter of the study was the volume fraction and aspect ratio of the fibers. It was found out that inclusion of fibers in concrete improved the ultimate torsional strength and imparted considerable ductility and toughness. The strength and toughness of beams were found to increase with increasing volume fraction and aspect ratio. A comparison of test results with torsion theories indicated that satisfactory prediction of ultimate torque could be obtained by using plastic theory.

Al-Ta'an and Al-Feel [9] proposed a method to calculate the ultimate shear strength of fiber-reinforced concrete rectangular beams without stirrups. The method showed a good agreement with published test results of 89 beams, which failed in shear. The data obtained from the

experiments were used in a regression analysis to identify the factors influencing the shear strength of fiber-concrete beams. Those factors were found to be the shear span-to-depth ratio, main reinforcement ratio, compressive strength of concrete and the fiber volume, dimensions, and type. Two formula were presented to predict the cracking and ultimate shear strength. Those formulas showed a good agreement with the experimental results.

Kim et. al. [27] studied the shear behavior of SFRC members without transverse reinforcement, and proposed a model based on a smeared crack model. The model were verified against experimental results showed a good agreement. The proposed shear behavior model has a clear theoretical basis, and ban be applied to steel fiber-reinforced concrete member as well as any other fiber-reinforced concrete members, when necessary, with a simple bond strength test. In general, the proposed model can capture the shear behavior of SFRC panels and shear strength of SFRC beams.

Purkiss and Wilson [28] proposed formulas to determine the load carrying capacity of beams and conduct the load-deflection curves. Results showed a very good correlation between the proposed formula and the experimental data for beams with and without steel fibers. It also showed a good agreement between the observed and calculated loads at crack initiation. A reasonable correlation was noted between the observed and calculated strain before cracking commenced. The correlation was less good post-cracking, although, still acceptable.

Ziara [10] initiated an experimental test program consisting of nine beams to study the influence of SF overlays on RC beams. It was found out that beams strengthened by SF overlays exhibited a remarkable increasing in load carrying capacity, aside from the ductility enhancement. Besides, mechanically bonded overlays showed better performance, where beams were able to reach their fully flexural capacity without inter-laminar shear failure.

From the aforementioned literature review, it is clear that most studies dealt mainly the mechanical properties of steel fiber reinforced concrete like load carrying capacity, shear behavior, behavior of SFRC beams in pure tension, and focused on developing mathematical models of stress-strain curve, load carrying capacity and other properties. Hence, the need for a research to study the behavior of SFRC beams numerically using finite element method becomes urgent.

Chapter 3
Numerical Modeling of Reinforced Concrete Material

Reinforced concrete (RC) structures exhibit a complex behavior even for low load levels. Non-linear compressive stress-strain relations, tensile cracking, post cracking, softening and interaction effects between concrete and reinforcing bars are the main sources of a highly nonlinear and complicated response. In order to capture the real structural behavior, sophisticated numerical tools are necessary to take into account all the remarkable phenomena and to perform the time-consuming non-linear calculations. For the last decade, a significant progress in formulating reinforced concrete material models was achieved, which widen the range and the scope of the nonlinear analysis to include more advance loading case such as triaxial loaded structures like offshore structures, floating vessels, submerged structures, dams and many other. Yet, developing material models of reinforced concrete under certain loading condition remain a big challenge, which limit the numerical analysis applicability.

3.1 Nonlinear behavior of reinforced concrete under monotonic loading

Modern Computation techniques like the finite element method have been used in nonlinear analysis of reinforced concrete structures for more than a decade. Reinforced concrete has a very complex behavior, involving such phenomena as inelasticity, crack and interactive effect between concrete and reinforcement.

Under increasing load, the following sequence of events takes place:

1. At low loads, the beam acts essentially as an uncracked elastic member.
2. Vertical flexural cracks then occur at midspan, resulting in a redistribution of stress and causing increase in steel stresses, bond stresses, and some bond slip.
3. Under additional load, these flexural cracks spread, increase, and if shear and diagonal tension are not critical, the beam eventually fails by yielding of the longitudinal tensile steel reinforcement or by crushing of the concrete in the compression zoon.
4. If shear and diagonal tension are critical, a much more complex situation evolves due to the formation of a significant diagonal-tension crack. This crack activates resistance to vertical shear by dowel action in the main longitudinal reinforcement, aggregate interlock

along the diagonal crack, stresses in vertical stirrups, and resistance in the uncracked concrete above the head of the crack.

5. A sudden increase in the longitudinal steel stress at the base of the diagonal-tension crack also occurs.
6. Under increasing load, the diagonal crack propagates toward the loading point, causing an increase in the dowel shear.
7. Final failure may occur when the head of the diagonal crack has decrease the uncracked compression block of concrete to a critical point, when shear-compression failure occurs under a combined state of stress. In some beams without stirrups, failure may occurs by splitting along the longitudinal reinforcement caused by the heavy dowel shear in the main reinforcement [11].

Most finite element studies consider concrete to act like an elasto-plastic solid in compression and like elastic brittle material in tension. Various elasticity – and plasticity – based constitutive models have been proposed for uncracked concrete. For cracking concrete, two different approaches have been employed for modeling. The most popular procedure is to treat cracking as distributed cracks on the continuum level; i.e., the cracks are smeared out in a continuous fashion. An alternative to the continuous model is the introduction of discrete cracks, which are traced individually as they progressively alter the topology of the structure. Since steel reinforcement is comparatively thin, it is generally assumed capable of transmitting axial force only; thus, a uniaxial stress-strain relationship is sufficient for general use [29].

In general, a full bond is assumed between the reinforcement and the concrete components, implying compatible deformation. Because of this assumption, the material stiffness of the composite element is obtained by superimposing material stiffnesses of the individual material components, concrete and reinforcement. In special cases, differential movements have been modeled, link-type element simulating bond slip between reinforcement and concrete. The material properties of steel reinforcement bars are easily established in uniaxial testing. The material properties are normally defined in using classical plasticity formulations. The reinforcement bars are usually incorporated in the computation model using discrete bar elements. Alternatively, by introducing equivalent layers. The bending rigidity of the bars is normally neglected [13].

In modeling the interaction between concrete and reinforcement, two important mechanisms have been identified. In the first type, the reinforcement and the concrete are both subjected to tension, so that large cracks form. The shear forces at the contact surface feed tension stresses into the concrete between the cracks. The concrete hangs on the bar and contributes to the overall stiffness of the system. This stiffness effect, often called tension stiffening, may be quite significant for concrete beams under normal working loads. It be accounted for in an indirect way by assuming a gradual loss of tension strength in concrete, or by special spring-type material models. Alternatively, by a more involved model for the interaction.

In the second type of interaction between the reinforcement and the concrete, there is a major shear deformation after tension cracking has first occurred. The bars act as dowels under such conditions. This dowel effect can be incorporated into a continuum model by using an equivalent shear stiffness and shear strength for the cracked concrete. A similar procedure can be applied for the aggregate inter-locking effect [30].

3.2 Concrete Material Models

Various mathematical models of the mechanical behavior of concrete are currently in use to analyze reinforced concrete structures. These can be divided into four main categories:

1. Orthotropic models
2. Nonlinear elasticity models
3. Plastic models
4. Endochronic models [13]

The simplest one of the aforementioned models is the orthotropic model. It was found that results of this model matches to a high point of accuracy the experimental data under proportional biaxial loading. The model was also found to be capable of predicting the hysteretic behavior of concrete under cyclic loading [31]. In beams, were the stress state is predominantly biaxial, the orthotropic model was found to be most suitable for analysis, and this includes panels and shells, as well.

The nonlinear elasticity model is based on the concept of variable moduli. It matches well several experimental data. In the pre-failure regime, unique approximate relationships have been established between hydrostatic and volumetric strain and between deviatoric stress and strain.

Derivation of tangent bulk and shear modulus can be done based on those relationships. Hence, the model is relatively simple and suitable for finite element computation. It also can predict the behavior of reinforced concrete when unloading takes place. A main flaw to this model is the continuity problem for the stress paths near neutral loading. Consequently, this model would not accurately describe the behavior of concrete under high stress, near the compressive strength, and in the strain softening range.

The strain hardening plastic model can be considered as a generalization of the orthotropic model and the nonlinear elasticity model. The formulation of constitutive relations are based on three fundamental assumptions:

1. The shape of the initial yield surface
2. The evolution of the loading surface
3. Formulation of a flow rule

Even though this model represents successfully the behavior in the strain-hardening region, the strain softening behavior of concrete beyond the peak stress cannot be described accurately by the classical theory of work-hardening plasticity. Therefore, it is not suitable to model reinforced concrete structures experience strain softening [32].

On the other hand, the Endochronic theory of plasticity is based on the concept of intrinsic time. The intrinsic time is used to measure the extent of damage in the internal structure of the concrete material under general deformation histories. The main flaw of this method is the expensive computation time, which limits its ability to be used to model large-scale structures [13].

For most beams and slabs subjected to bending moments, a biaxial stress state controls the overall stress formation. The stress developed in the beam mainly lies in the tension-tension or compression-compression region and only a small portion near the supports lie in the compression-tension region.

3.3 Concrete Failure Surface

Current and most used FEM codes analyze reinforced concrete under multiaxial stress, in which, the concrete element would be subjected to tension/compression in the three-principle direction.

One of the most reliable failure criterion of concrete under triaxial load is William-Warnke five parameters failure criterion [33]. The failure surface will be considered throughout this thesis. It can be expressed in the form:

$$\frac{F}{f_c} - S \geq 0 \qquad \textbf{[Eq. 3-1]}$$

Where:

- F = a function of the principal stress state (σ_{xp}, σ_{yp}, σ_{zp})
- S = failure surface expressed in terms of principal stresses and five input parameters:
  - f_t: Ultimate uniaxial tensile strength
  - f_c: Ultimate uniaxial compressive strength
  - f_{cb}: Ultimate biaxial compressive strength
  - f_1: Ultimate compressive strength for a state of biaxial compression superimposed on hydrostatic stress state
  - f_2: Ultimate compressive strength for a state of uniaxial compression superimposed on hydrostatic stress state
- f_c = uniaxial crushing strength
- σ_{xp}, σ_{yp}, σ_{zp} = principal stresses in principal directions

However, the failure surface can be simplified with a minimum of two parameters, f_t and f_c. The other three parameters would be:

- $f_{cb} = 1.20 \times f_c$ **[Eq. 3-2]**
- $f_1 = 1.450 \times f_c$ **[Eq. 3-3]**
- $f_2 = 1.725 \times f_c$ **[Eq. 3-4]**

However, these default values are valid only for stress states where the condition: $|\sigma_h| = \sqrt{3} \times f_c'$ is satisfied, where σ_h is the hydrostatic stress state = 1/3 (σ_{xp} + σ_{yp} + σ_{zp}). Both the function "*F*" and the failure surface "S" are expressed in terms of principal stresses denoted as σ_1, σ_2, and σ_3 where:

- $\sigma_1 = \max(\sigma_{xp}, \sigma_{yp}, \sigma_{zp})$ **[Eq. 3-5]**
- $\sigma_3 = \min(\sigma_{xp}, \sigma_{yp}, \sigma_{zp})$ **[Eq. 3-6]**

Based on the values of σ_1, σ_2, σ_3 the failure of concrete can be categorized into four domains:

1. $0 \geq \sigma_1 \geq \sigma_2 \geq \sigma_3$ (compression - compression - compression)
2. $\sigma_1 \geq 0 \geq \sigma_2 \geq \sigma_3$ (tensile - compression - compression)
3. $\sigma_1 \geq \sigma_2 \geq 0 \geq \sigma_3$ (tensile - tensile - compression)
4. $\sigma_1 \geq \sigma_2 \geq \sigma_3 \geq 0$ (tensile - tensile - tensile)

3.3.1 The Domain (Compression - Compression - Compression)

In the "compression–compression–compression" regime, the failure criterion of Willam and Warnke is implemented. In this case, "F" takes the form:

$$F = F_1 = \frac{1}{\sqrt{15}}[(\sigma_1 - \sigma_2)^2 + (\sigma_2 - \sigma_3)^2 + (\sigma_3 - \sigma_1)^2]^{1/2} \quad \textbf{[Eq. 3-7]}$$

and "S" is defined as:

$$S = S_1 = \frac{2r_2(r_2^2 - r_1^2)\cos\mu + r_2(2r_1 - r_2)[4(r_2^2 - r_1^2)\cos_\mu^2 + 5r_1^2 - 4r_1r_2]^{1/2}}{4(r_2^2 - r_1^2)\cos_\mu^2 + (r_2 - r_1)^2} \quad \textbf{[Eq. 3-8]}$$

Where:

$$\cos\mu = \frac{2\sigma_1 - \sigma_2 - \sigma_3}{\sqrt{2}[(\sigma_1 - \sigma_2)^2 + (\sigma_2 - \sigma_3)^2 + (\sigma_3 - \sigma_1)^2]^{1/2}} \quad \textbf{[Eq. 3-9]}$$

$r_1 = a_0 + a_1\zeta + a_2\zeta^2$ **[Eq. 3-10]**

$r_2 = b_0 + b_1\zeta + b_2\zeta^2$ **[Eq. 3-11]**

$\zeta = \sigma_h / f_c'$ **[Eq. 3-12]**

As shown in **Figure 3-9**, the failure surface appears to have a cyclic symmetry about each 120 sector of the octahedral plan. The value of r_1 is evaluated based on the constant values a_0, a_1, and a_2 values. While, r_2 is evaluated based on the constant values of b_0, b_1, and b_2.

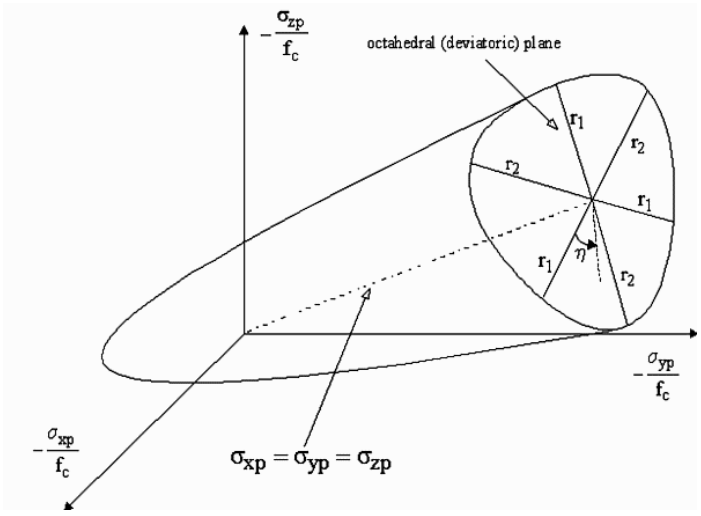

Figure 3-9: Willam-Warnke 3-D Failure Surface in Principal Stress Space *[33]*

Those coefficients can be evaluated by solving the following equations, simultaneously.

$$\begin{Bmatrix} \frac{F_1}{f_c'}(\sigma_1 = f_t, \sigma_2 = \sigma_3 = 0) \\ \frac{F_1}{f_c'}(\sigma_1 = 0, \sigma_2 = \sigma_3 = -f_{cb}) \\ \frac{F_1}{f_c'}(\sigma_1 = -\sigma_h^a, \sigma_2 = \sigma_3 = -\sigma_h^a - f_1) \end{Bmatrix} = \begin{bmatrix} 1 & \zeta_t & \zeta_t^2 \\ 1 & \zeta_{cb} & \zeta_{cb}^2 \\ 1 & \zeta_1 & \zeta_1^2 \end{bmatrix} \begin{Bmatrix} a_0 \\ a_1 \\ a_2 \end{Bmatrix} \quad \textbf{[Eq. 3-13]}$$

$$\begin{Bmatrix} \frac{F_1}{f_c'}(\sigma_1 = \sigma_2 = 0, \sigma_3 = -f_c) \\ \frac{F_1}{f_c'}(\sigma_1 = \sigma_2 = -\sigma_h^a, \sigma_3 = -\sigma_h^a - f_2) \\ \frac{F_1}{f_c'}(0) \end{Bmatrix} = \begin{bmatrix} 1 & -1/3 & 1/9 \\ 1 & \zeta_2 & \zeta_2^2 \\ 1 & \zeta_0 & \zeta_0^2 \end{bmatrix} \begin{Bmatrix} b_0 \\ b_1 \\ b_2 \end{Bmatrix} \quad \textbf{[Eq. 3-14]}$$

Where:

- $\zeta_t = \frac{f_t}{3f_c}$ **[Eq. 3-15]**
- $\zeta_{cb} = -\left(\frac{2f_{cb}}{3f_c}\right)$ **[Eq. 3-16]**
- $\zeta_1 = -\left(\frac{\sigma_a^h}{f_c}\right) - \left(\frac{2f_1}{3f_c}\right)$ **[Eq. 3-17]**
- $\zeta_2 = -\left(\frac{\sigma_a^h}{f_c}\right) - \left(\frac{f_2}{3f_c}\right)$ **[Eq. 3-18]**

And ζ_0 is the positive root of the following equation: $a_0 + a_1\zeta_0 + a_2\zeta_{02} = 0$ **[Eq. 3-19]**

For all the aforementioned equations, if the failure surface $\frac{F}{f_c} - S \geq 0$ is satisfied, the material is assumed to crush.

3.3.2 The Domain (Tension - Compression - Compression)

In the "Tension – Compression – Compression" regime, "F" is taken as:

$$\frac{1}{\sqrt{15}}[(\sigma_2 - \sigma_3)^2 + (\sigma_2)^2 + (\sigma_3)^2]^{1/2} \quad \textbf{[Eq. 3-20]}$$

and "S" is defined by:

$$(1 - \frac{\sigma_1}{f_t}) \frac{2P_2(p_2^2 - p_1^2)\cos\mu + p_2(2p_1 - p_2)[4(p_2^2 - p_1^2)\cos_\mu^2 + 5p_1^2 - 4p_1p_2]^{1/2}}{4(p_2^2 - p_1^2)\cos_\mu^2 + (p_2 - p_1)^2} \quad \textbf{[Eq. 3-21]}$$

Where:

- $p_1 = a_0 + a_1x + a_2x^2$ **[Eq. 3-22]**
- $p_2 = b_0 + b_1x + b_2x^2$ **[Eq. 3-23]**
- $x = (\sigma_2 + \sigma_3)/3f_c$. **[Eq. 3-24]**

If the failure criterion is satisfied, cracking occurs in the plane perpendicular to principal stress σ_1.

3.3.3 The Domain (Tension - Tension - Compression)

In the "tension – tension – compression" regime, "F" takes the form: $F = \sigma_i$, where i = 1, 2 and "S" is defined as $S = (f_t/f_c) \times (1 + (\sigma_3/f_c))$. If the failure criterion for both i = 1, 2 is satisfied,

cracking occurs in the planes perpendicular to principal stresses σ_1 and σ_2. If the failure criterion is satisfied only for $i = 1$, cracking occurs only in the plane perpendicular to principal stress σ_1.

3.3.4 The Domain (Tension - Tension - Tension)

In the "tension – tension – tension" regime, "F" takes the form: $F = \sigma_i$, where i = 1, 2, 3 and "S" is defined as $S = f_t/f_c$. If the failure criterion is satisfied in directions 1, 2, and 3, cracking occurs in the planes perpendicular to principal stresses σ_1, σ_2, and σ_3. If the failure criterion is satisfied in directions 1 and 2, cracking occurs in the plane perpendicular to principal stresses σ_1 and σ_2. If the failure criterion is satisfied only in direction 1, cracking occurs in the plane perpendicular to principal stress σ_1.

3.4 Behavior of Concrete Cracked Section

The major factor affects the behavior of reinforced concrete is the progressive cracking. Cracking of concrete contributes significantly to its nonlinearity under loading and leads to a localized failure, which will lead eventually to a total failure of the structural element.

When cracks take place, the tensile stress is carried out entirely by the reinforcing steel. Tensile stresses are, however, present in the concrete between the cracks, since some tension is transferred from steel to concrete through bond. The magnitude and distribution of bond stresses between the cracks determines the distribution of tensile stresses in the concrete and the reinforcing steel between the cracks. Additional cracks can form between the initial cracks, if the tensile stress exceeds the concrete tensile strength between previously formed cracks. The final cracking state is reached when a tensile force of sufficient magnitude to form an additional crack between two existing cracks can no longer be transferred by bond from steel to concrete.

When concrete reaches its tensile strength, cracks at location of maximum tensile stress start to form. The number, locations, and extent of cracks are dependent on the size and location of reinforcing steel. At the initial cracks, concrete stress drops to zero and the steel carries the entire tensile force. However, the concrete between the cracks still carries some tensile stress, which decreases with increasing applied load. This drop in concrete tensile stress could be attributed to the progressive deterioration in bond between concrete and reinforcement, where a secondary

system in internal cracks start to form around the reinforcing bars, those cracks are called “bond cracks” [34].

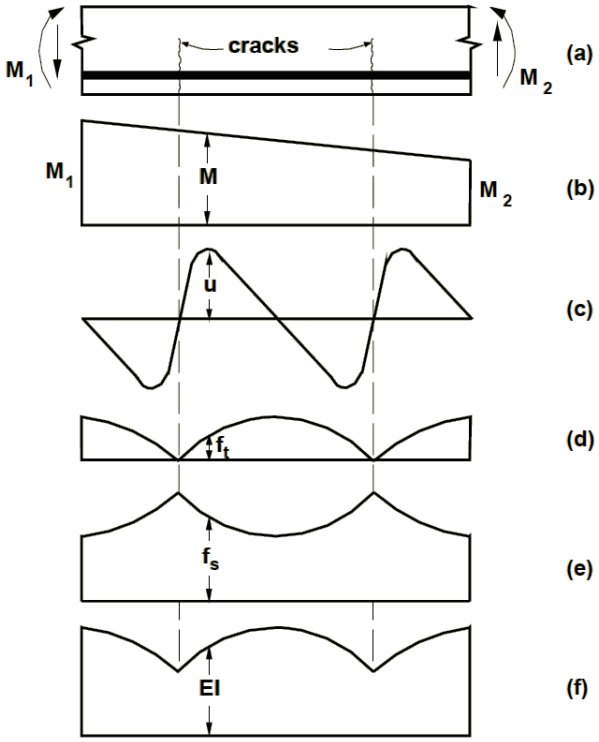

Figure 3-10: (a) portion of beam, (b) bending moment distribution, (c) bond stress distribution, (d) concrete tensile stress distribution, (e) steel tensile stress distribution, (f) flexural stiffness distribution in elastic range [34]

3.5 Crack Models

Tensile failure in matrix-aggregate composites like concrete involves progressive micro-cracking, tortuous debonding and other process of internal damage. These softening processes eventually coalesce into a geometrical discontinuity that separates the material. Such discontinuity is called a crack. Cracks developing in concrete during the loading phase can be modeled by one of the following:

1. Discrete crack model
2. Smeared crack model

Undoubtedly, the discrete crack concept is the approach that reflects this phenomenon most closely. It models the crack directly via a displacement-discontinuity in an interface element that

separates two solid elements. Unfortunately, the approach does not fit the nature of the finite element displacement method and it is computationally more convenient to employ a smeared crack concept. A smeared crack concept imagines the cracked solid to be a continuum and permits a description in terms of stress-strain relation. However, here the converse drawback occurs, since the underlying assumption of displacement continuity conflicts with the realism of the geometrical discontinuity [35].

3.5.1 Discrete crack model

The discrete crack model assumes a separation between element edges. The approach suffers from two drawback. First, it implies a continuous change in nodal connectivity, which does not fit the nature of the finite element displacement method. Secondly, the crack is constrained to follow predefined path along the element edges. A class of problems exists, however, whereby the orientation of the discrete crack is not necessarily the prime subject of interest. One may think of fracture in the form of a straight separation band, the location of which is known in advance, or of discrete cracks along the interface between concrete and reinforcement. Furthermore, engineering problems exist whereby a mechanism of discrete cracks can be imagined to occur in a fashion similar to yield line mechanisms. For suck cases, the above drawbacks vanish and one may use a simple form of discrete cracks with a predefined orientation.

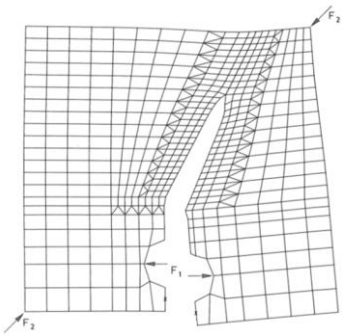

Figure 3-11: Change in Topology of Finite Elements [35]

With the change of topology and the redefinition of nodal points, the narrow bandwidth of the stiffness matrix is destroyed and a greatly increased computational effort results in this model. Moreover, the lack of generality in crack orientation has made the discrete crack model unpopular. In spite of these shortcomings, the use of discrete crack models in finite element analysis offers

certain advantages over the other methods. For those problems that involve a few dominant cracks, the discrete crack approach offers a more realistic description of the cracks, which represent strain discontinuities in the structure. Such discontinuities are correctly characterized by the discrete crack model [35].

3.5.2 Smeared Crack Model

The need for a crack model that offers automatic generation of cracks and complete generality in crack orientation, without the need of redefining the finite element topology, has led the majority of investigators to adopt the smeared crack model. Rather than representing a single crack, the smeared crack model represents many finely spaced cracks perpendicular to the principal stress direction. This approximation of cracking behavior of concrete is quite realistic, since the fracture behavior of concrete is very different from that of metals. In concrete fracture is preceded by microcracking of material in the fracture process zone, which manifests itself as strain softening. This zone is often very large relative to the cross section of the member due to the large size of aggregate.

With this continuum approach, the local displacement discontinuities at cracks are distributed over some tributary area within the finite element. In contrast to the discrete crack concept, the smeared crack concept fits the nature of the finite element displacement method, since the continuity of the displacement field remains intact.

Although this approach is simple to implement and is, therefore, widely used. It has nevertheless a major drawback, which is the dependency of the results on the size of the finite element mesh used in the analysis. When large finite elements are used, each element has a large effect on the structural stiffness. When a single element cracks, the stiffness of the entire structure is greatly reduced. Higher order elements in which the material behavior is established at a number of integration points do not markedly change this situation, because, in most cases, when a crack takes place at one integration point, the element stiffness is reduced enough so that a crack will occur at all other integration points of the element in the next iteration. Thus, a crack at an integration point does not relieve the rest of the material in the element, since the imposed strain continuity increases the strains at all other integration points. The overall effect is that the

formation of a crack in a large element results in the softening of a large portion of the structure. The difficulty stems from the fact that a crack represents a strain discontinuity, which cannot be modeled correctly within a single finite element in which the strain varies continuously [32].

Smeared crack models can be categorized into: 1. Fixed smeared crack model, 2. Rotating smeared crack model. The Orientation of a crack in the fixed smeared crack model is fixed during the entire computational process. While, a rotating smeared crack model allows the orientation of the crack to co-rotate with the axes of principal strain [35].

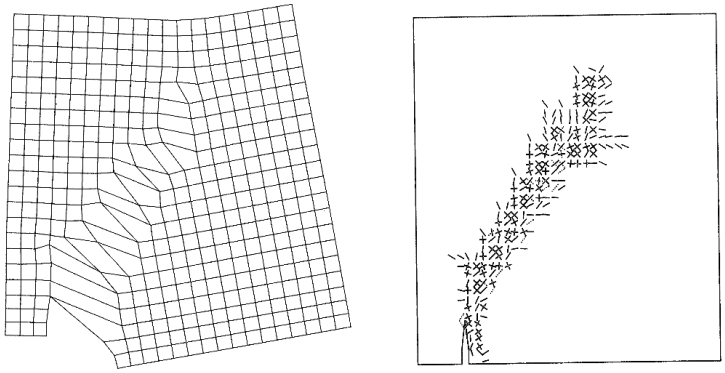

Figure 3-12: Fixed Crack Model [35]

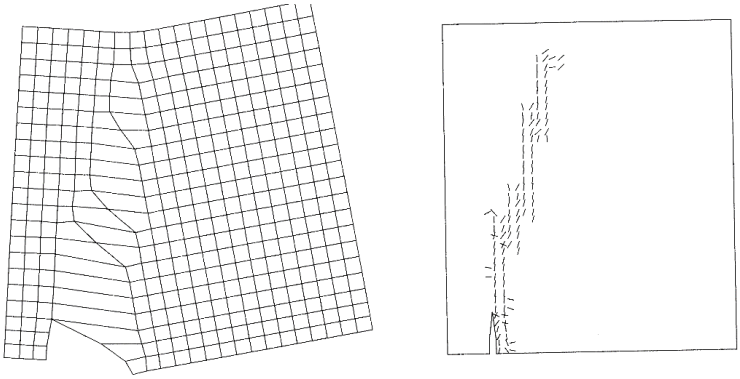

Figure 3-13: Rotated Crack Model [35]

3.6 Reinforcing Steel Models

Modeling steel reinforcement is much easier than modeling concrete since it is not environmental conditions or time dependent. A uniaxial stress-strain relationship would suffice to define the

material properties needed to carry out the analysis of reinforced concrete structures. For practical purposes, reinforcing steel exhibit the same behavior in tension as in compression, as showing in **Figure 3-14**. The behavior of steel exhibits a linear elastic behavior. Since steel reinforcement is used in concrete construction in the form of reinforcing bars or wire, it is not necessary to introduce the complexities of three-dimensional constitutive relations for steel. For computational convenience, it even often suffices to idealize the one dimensional stress-strain relation for steel.

Reinforcing steel can be modeled as:

1. Smeared model
2. Embedded model
3. Discrete model

In the Smeared model, the reinforcing steel is assumed to be distributed over the concrete element at a certain orientation angle. A composite concrete-steel constitutive relation is used in this case, which, however, requires that perfect bond be assumed between concrete and steel. An embedded steel model is useful in connection with higher order isoparametric concrete elements. The reinforcing steel is considered as an axial member built into the isoparametric element such that its displacements are consistent with those of the element. Such a model again implies perfect bond between concrete and steel. A drawback to this model is the high computational effort and time required to the analysis. The most widely used model represents the reinforcement with discrete one-dimensional truss elements, which are assumed to be pin connected and possess two degrees of freedom at each node. Alternatively, beam elements can also be used, in which case, three degrees of freedom are allowed at each end of the bar element. In either case, the one-dimensional reinforcing bar elements can be easily superimposed on the two-dimensional concrete element mesh. A significant advantage of the discrete representation, in addition to its simplicity, is that it can include the slip of reinforcing steel with respect to the surrounding concrete.

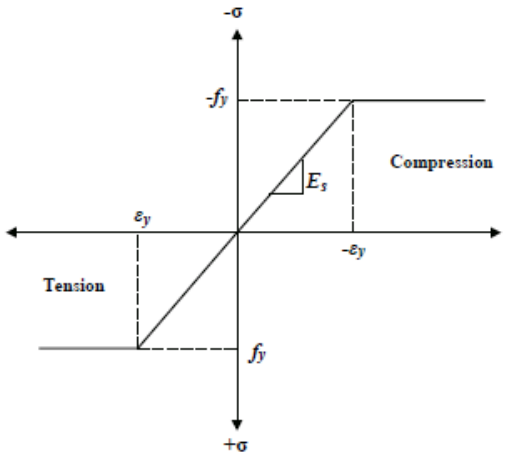

Figure 3-14: Idealized Stress-Strain Relationship of Reinforcing Steel

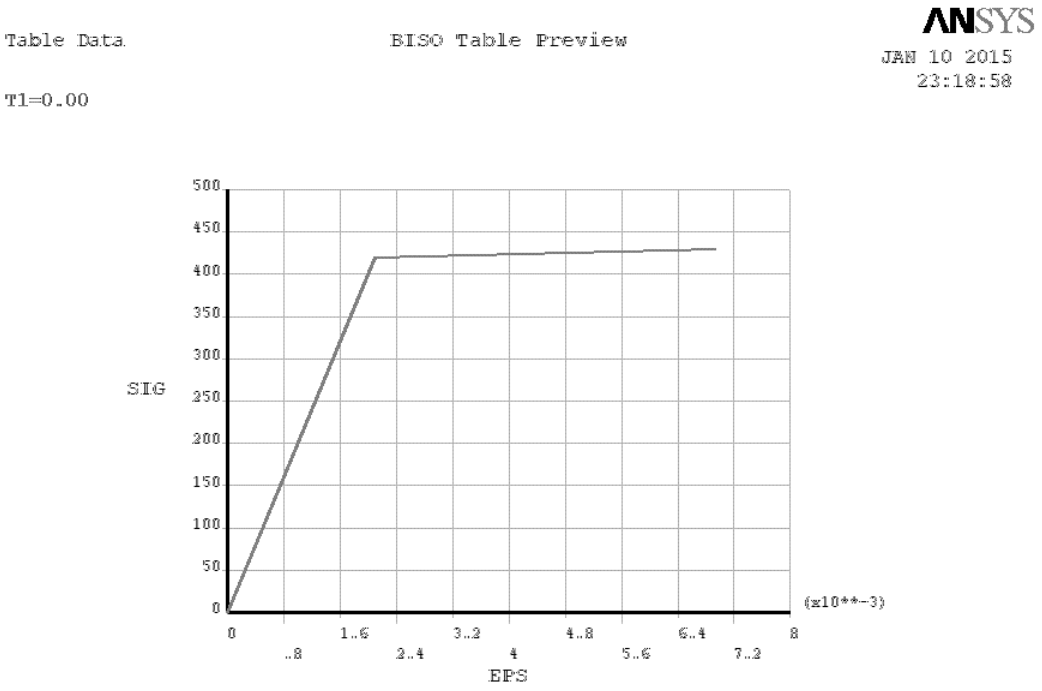

Figure 3-15: Linear Elastic-Perfect Plastic Model (ANSYS MATERIAL DESCRIPTION)

Chapter 4
Case Study

4.1 Introduction

This chapter contains a comprehensive description of the numerical models, i.e., material models, failure criterion for ordinary concrete, SFRC and reinforcing steel, elements to be used, loading inputs, constraints and numerical solvers. The results of the numerical models analysis will be presented in the next chapter.

4.2 Finite Element Modeling

Over the years, different methods have been utilized to study the response of structural elements, and predict their failure load. Analytical, as well experimental programs have been used to analyze and study the response of different individual elements under loading. Although, experimental tests method represents real life response, it is time consuming and costly to some level. Finite element method has been used to study the structural elements and its response to the imposed loads. Early attempts to do so were time-consuming and infeasible. In recent years, however, the use of FEM increased due to progressing knowledge and capabilities of computers software and hardware. However, despite the proliferation of FE packages, and steadily increasing adoption of the technique for the solution of nonlinear structural problems, FEM has not met, to date, with widespread success in the case of reinforced concrete. This is due to two reasons, the first is the direct consequence of unrealistic material description, and the other is the computational problems that arise because of numerical instabilities associated with cracking of concrete. Nonetheless, several constitutive models have been proposed in the recent years to represent reinforced concrete, where satisfactory results obtained in comparison to the experimental based tests.

To investigate the behavior of RC beams strengthened with SFRC overlays, the well-known FE package ANSYS APDL v13.0 has been used. ANSYS presenting various types of isoparametric elements to model both steel and concrete. Those elements came with both linear and nonlinear material description.

4.3 Model Description

To study the behavior of RC beams strengthened with SFRC overlay, a set of numerical models have been investigated. These models will be verified later against experimental data to assure the eligibility of the FEM code. The numerical program consist of three beams, Beam B1-FEM modeled using an ordinary concrete material description. Beam F1-FEM will be modeled twice. Once using a smeared SFRC model, and the other one using a discrete SFRC mode. Beam S4-FEM modeled with half cross-section of an ordinary material description and the other half of cross-section with SFRC material description. Beam S4 have two arrangements; the first one is with SFRC overlay, while the other one is with SFRC underlay. For comparison purposes, all beams have the same geometrical properties, with overall length of 2000mm and width to depth dimension of 150mm × 200 mm. Longitudinal flexural reinforcement was modeled using 2Ø-14 mm nominal diameter deformed steel bars. Meanwhile, the secondary reinforcement was modeled using 2Ø-8 mm placed on the compression side of the beam. The stirrups were modeled using 2Ø-8mm nominal diameter.

A control beam of ordinary concrete BEAM B1 were modeled for comparison reasons and considered as a *Control Beam*. This beam is of a tension-control section, and it was design in a ductile manner and reached its full flexural capacity. BEAM F1 is an identical replica of BEAM B1, except it was modeling as SFCR beam.

BEAM S4 consist of two parts, the ordinary concrete part, and the SFRC overlay and underlay part. The beam length and width are similar to BEAM B1 and F1, except the depth of the ordinary concrete is 120 mm, while the SFRC overlay\underlay is 120 mm.

The following table summarize the beams' both geometrical and material properties:

		B1-FEM	**F1-FEM**	**S4-FEM-OL OVERLAY**	**S4-FEM-UL UNDERLAY**
Geometry	Length (mm)	2000	2000	2000	2000
	Width (mm)	150	150	150	150
	Depth (mm)	240	240	120 OC 120 OVERLAY	120 OC 120 UNDERLAY
	Loading System	4 Pt.	4 Pt.	4 Pt.	4 Pt.
	Shear Span (mm)	562.5	562.5	562.5	562.5
	Effective depth (mm)	215	215	215	215
	ø (Bottom Long. Bars) (mm)	14	14	14	14
	ø (Top Long. Bars) (mm)	8	8	8	8
	ø (Stirrups) (mm)	8	8	8	8

		B1-FEM	F1-FEM	S4-FEM-OL OVERLAY	S4-FEM-UL UNDERLAY
Material	*f*c' (MPa)	25.2	26	25 SFRC (21.5)	25 SFRC (21.5)
	*f*y (MPa)	410	410	410	410
	*f*y – Stirrups (MPa)	280	280	280	280

Table 1: Geometrical and Material Properties of Numerical Beams

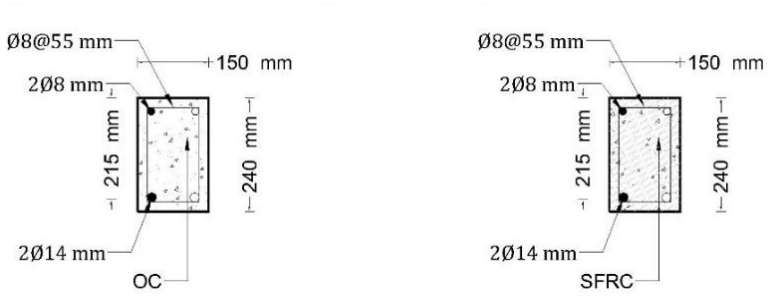

Figure 4-16: Beam B1 (LEFT), Beam F1 (RIGHT)

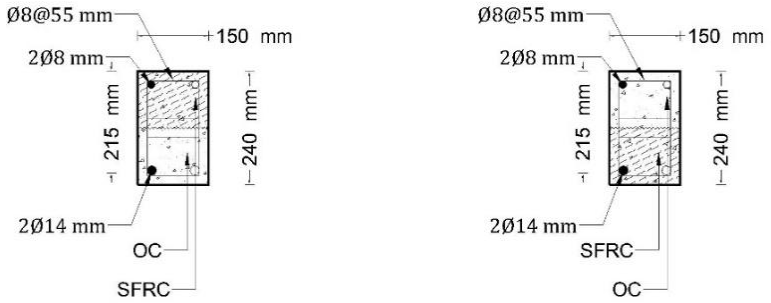

Figure 4-17: Beam S4 Overlay (LEFT), Beam S4 Underlay (RIGHT)

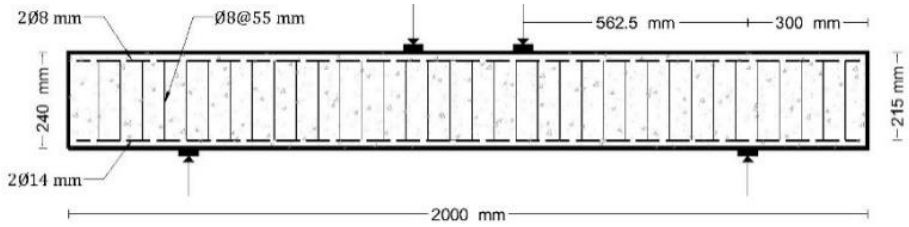

Figure 4-18: Beam B1 - Ordinary Concrete

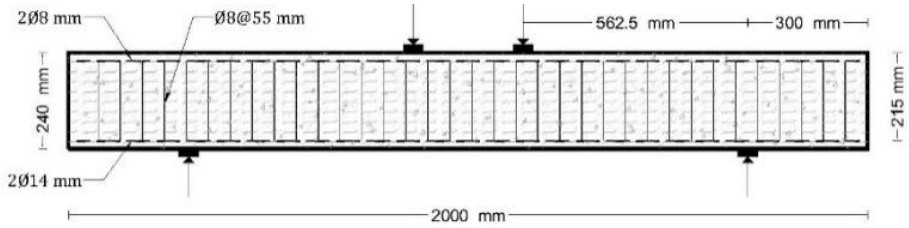

Figure 4-19: Beam F1 - SFRC Beam

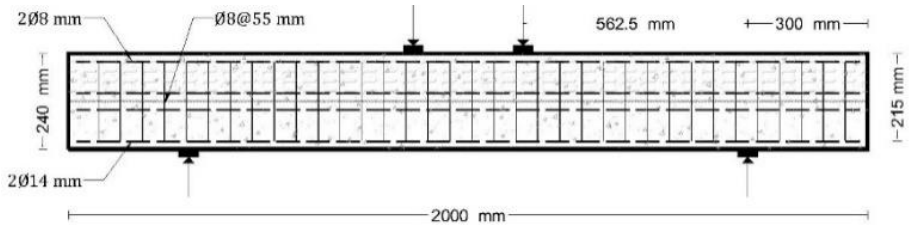

Figure 4-20: Beam S4 (Overlay)

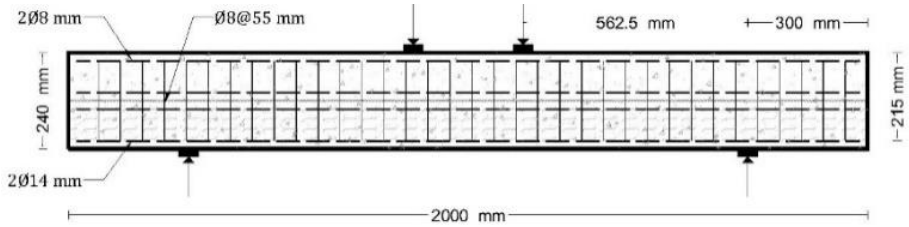

Figure 4-21: Beam S4 (Underlay)

4.4 Concrete Modeling

ANSYS presenting element *SOLID65* to model concrete. SOLID65 is used for the 3-D modeling of solids with or without reinforcing bars (rebar). The SOLID65 is capable of cracking in tension and crushing in compression. In concrete applications, for example, the SOLID65 capability of the element may be used to model the concrete while the rebar capability is available for modeling reinforcement behavior. The element is defined by eight nodes having three degrees of freedom at each node: translations in the nodal x, y, and z directions. Up to three different rebar specifications may be defined. The concrete element is similar to a 3-D structural solid but with the addition of special cracking and crushing capabilities. The most important aspect of this element is the treatment of nonlinear material properties. The concrete is capable of cracking (in three orthogonal directions), crushing, plastic deformation, and creep. The rebar are capable of tension and compression, but not shear. They are also capable of plastic deformation and creep.

The geometry, node locations, and the coordinate system for this element are shown in **Figure 4-22**. The element is defined by eight nodes and isotropic material properties. The element has one solid material and up to three rebar materials. The volume ratio is defined as the rebar volume divided by the total element volume. The orientation is defined by two angles (in degrees) from the element coordinate system. A rebar material number of zero or equal to the element material number removes that rebar capability.

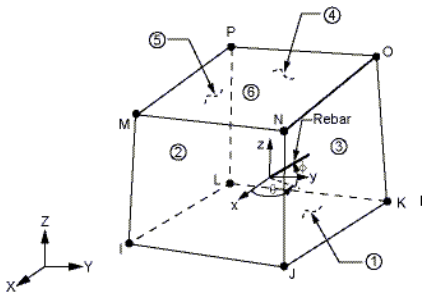

Figure 4-22: SOLID65 Geometry

Additional concrete material data, such as the shear transfer coefficients, tensile stresses, and compressive stresses are input in the data table. Typical shear transfer coefficients range from 0.0 to 1.0, with 0.0 representing a smooth crack (complete loss of shear transfer) and 1.0 representing a rough crack (no loss of shear transfer). This specification may be made for both the closed and open crack. When the element is cracked or crushed, a small amount of stiffness is added to the element for numerical stability. The stiffness multiplier CSTIF is used across a cracked face or for a crushed element, and defaults to 1.0E-6.

SOLID65 Assumptions and Restrictions

- Cracking is permitted in three orthogonal directions at each integration point.
- If cracking occurs at an integration point, the cracking is modeled through an adjustment of material properties, which effectively treats the cracking as a "smeared band" of cracks, rather than discrete cracks.
- The concrete material is assumed to be initially isotropic.
- Whenever the reinforcement capability of the element is used, the reinforcement is assumed to be "smeared" throughout the element.
- In addition to cracking and crushing, the concrete may also undergo plasticity, with the Drucker-Prager failure surface being most commonly used. In this case, the plasticity is done before the cracking and crushing checks.

4.4.1 Modeling of Ordinary Concrete Part of Beam

Ordinary concrete will be modeled using element "SOLID65". Linear and nonlinear material properties will be incorporated into the FE code. And since the discrete reinforcement model will be used, no smeared properties will be introduced in the ordinary concrete model.

4.4.2 Modeling of SFRC Overlay

Steel Fiber-Reinforced Concrete modeled using "SOLID65". Linear and nonlinear material properties have been incorporated into the FE code.

Modeling of steel fiber can be done by either way:

1. Smeared model: Assuming homogenous material properties of SFRC. In this case, the steel fiber effect will be smeared into the material properties.
2. Discrete model: the steel fibers will be modeled discretely using the smeared material properties for each of SFRC elements. The orientation of the steel fibers will be arbitrary to reflect the real-life situation.

Since the location and orientation of steel fibers are arbitrary, the smeared model will be adopted to represent the steel fibers for all beams. A homogenous material property of SFRC will be assumed. The steel fibers dosage as a volume fraction will set to 1.5%. The SFRC will have a higher tensile strength compared to ordinary concrete. The value of tensile strength for a volume fraction of 1.5% will be taken as 14-16% of compressive strength [24].

Moreover, both smeared and discrete model will be adopted for beam F1-FEM that will be modeled using SFRC material properties. Modeling beam F1-FEM with both models will be for comparison purposes.

Since both ordinary concrete and SFRC exhibit the same failure phenomenon, i.e. crushing in compression and cracking in tension, element SOLID65 will be used to model both materials and only the material description model will be different.

4.5 Concrete Material description

For concrete, linear and nonlinear material properties are required, as well the definition of the failure surface. Definition of linear material properties includes modulus of elasticity E_c, and Poisson's ratio v_c. ACI 8.5.1 design code proposes the following empirical equation to evaluate modulus of elasticity of normal weight concrete: $w_c^{1.5} \times 0.043\sqrt{f_c'}$. For the nonlinear part of the material properties, a stress-strain curve shall be defined. A very popular and reliable model of *Hognestad* will be used to describe the stress-strain relationship. This model consists of a second-

degree parabola with apex at a strain of $1.8f_c^{''}/E_c$, where $f_c^{''} = 0.9f_c^{'}$, followed by a downward-sloping line terminating at a stress of $0.85\,f_c^{'}$ and a limiting strain of 0.0038. The stress at any point can be evaluated using the formula: $f_c''\left(\frac{2\varepsilon_c}{\varepsilon_0} - \left(\frac{\varepsilon_c}{\varepsilon_0}\right)^2\right)$, where ε_0 equals $1.8f_c^{''}/E_c$ and ε_c represents strain at different stress values [16].

The linear behavior of the ordinary concrete is assumed to extend up to 30% of concrete compressive strength. Through the linear phase, Hooke's Law is assumed to be valid, hence, $\sigma = E\times\varepsilon$. Afterward, a nonlinear behavior of concrete takes place. "*Multilinear Isotropic Hardening Constants*" model presented by ANSYS would be most suitable. More stress-strain points would yield more satisfactory results, yet, would consume more time and computational effort. The slope of the first segment of the curve must correspond to the elastic modulus of the material and no segment slope should be larger. No segment can have a slope less than zero. The slope of the stress-strain curve is assumed to be zero beyond the last user-defined stress-strain data point, i.e., the apex of the stress-strain curve. Table 2 summarizes the concrete material properties.

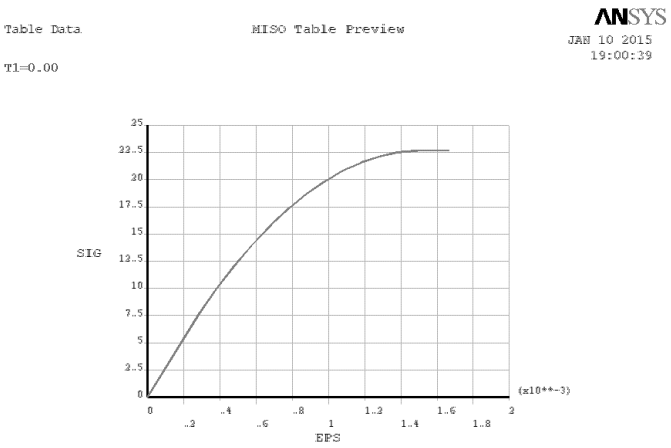

Figure 4-23: Multilinear Stress-Strain Curve for B1-FEM

In order to get a realistic response of concrete element and determine accurately the load failure, a failure criterion should be defined. ANSYS presents Willam-Warnke five parameters failure surface. This yield criterion has a conical shape with a curved meridians and noncircular base sections as well as nonaffine sections in the devatoric plan. This model is a modified one for a three parameters model of Willam-Warnke. It was proposed with two additional degrees of freedom for describing curved meridians to the elliptical type of noncircular cross section [33].

In this way, the failure surface of Willam-Warnke can be applied to low- as well as high-compression regimes, the five parameters are:

1. The uniaxial compressive strength, f_c.
2. The uniaxial tensile strength, f_t.
3. The equal biaxial compressive strength, f_{cb}.
4. The high-compression-stress point on the tensile meridian, f_1.
5. The high-compression-stress point on the compressive meridian, f_2.

Linear Properties

Property	B1	F1	S4 Overlay	
			Ordinary Concrete	SFRC Overlay\Underlay
v_c	0.3	0.3	0.3	0.3
E_c (MPa)	26982	27407	26875	24923

Nonlinear Properties

Point	B1		F1		S4			
					Ordinary Concrete		SFRC Overlay\Underlay	
	Strain (m/m)	Stress (MPA)	Strain (m/m)	Stress (MPA)	Strain (m/m)	Stress (MPA)	Strain (m/m)	Stress (MPA)
0.	0.00000	0.00	0.00000	0.00	0.00000	0.00	0.00000	0.00
1.	0.00028	7.56	0.00028	7.80	0.00028	7.50	0.00026	6.45
2.	0.00038	9.97	0.00033	9.08	0.00033	8.75	0.00031	7.61
3.	0.00048	12.11	0.00038	10.25	0.00038	9.90	0.00036	8.66
4.	0.00058	14.06	0.00043	11.36	0.00043	10.99	0.00041	9.66
5.	0.00068	15.81	0.00048	12.43	0.00048	12.03	0.00046	10.62
6.	0.00078	17.36	0.00053	13.45	0.00053	13.03	0.00051	11.53
7.	0.00088	18.71	0.00058	14.42	0.00058	13.97	0.00056	12.38
8.	0.00098	19.87	0.00063	15.34	0.00063	14.86	0.00061	13.19
9.	0.00108	20.82	0.00068	16.20	0.00068	15.71	0.00066	13.94
10.	0.00118	21.58	0.00073	17.02	0.00073	16.51	0.00071	14.65
11.	0.00128	22.14	0.00078	17.79	0.00078	17.25	0.00076	15.31
12.	0.00138	22.51	0.00083	18.51	0.00083	17.95	0.00081	15.92
13.	0.00148	22.67	0.00088	19.19	0.00088	18.59	0.00088	16.74
14.	0.00151	22.68	0.00098	20.38	0.00098	19.74	0.00096	17.44
15.			0.00108	21.37	0.00108	20.69	0.00103	18.04
16.			0.00118	22.17	0.00118	21.44	0.00111	18.52
17.			0.00128	22.77	0.00128	21.99	0.00118	18.90
18.			0.00138	23.17	0.00138	22.34	0.00126	19.16
19.			0.00148	23.37	0.00144	22.46	0.00131	19.27
20.			0.00154	23.40	0.00151	22.50	0.00140	19.35

Table 2: Stress-Strain Data for numerical models

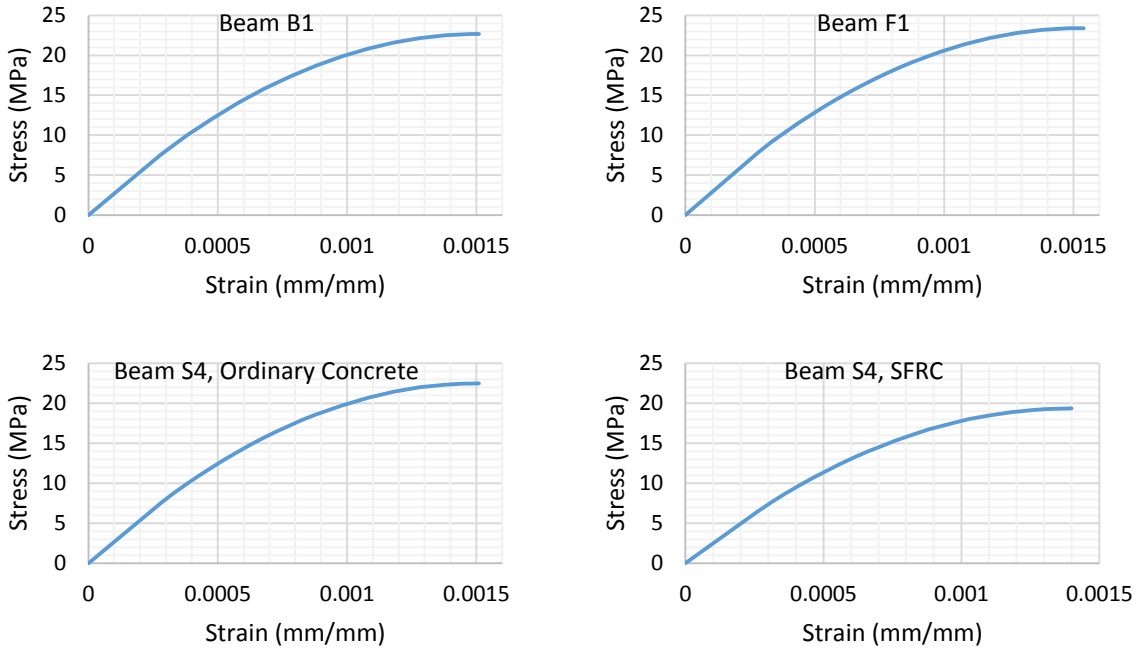

Figure 4-24: Stress-Strain curves for Beam "B1-FEM" (TOP-LEFT), Beam "F1-FEM" (TOP-RIGHT), Beam "S4-FEM-OL" – Ordinary Concrete Properties (BOTTOM-LEFT), Beam "S4-FEM-OL" – SFRC Properties

However, the failure surface can be specified with a minimum of two constants, f_t and f_c. The other three constants default to Willam and Warnke:

$$f_{cb} = 1.2 \times f_c$$
$$f_1 = 1.45 \times f_c$$
$$f_2 = 1.725 \times f_c$$

Along with the five parameters, an open and close crack retention factor must be defined. This transfer coefficient β_t represents a shear-strength reduction factor for those subsequent loads, which induce sliding (shear) across the crack face. The value of β_t varies from 0 to 1, with 0 representing no shear transfer (smooth crack) and 1 presenting a full shear transfer across the crack face (rough crack). A multiplier to account for amount of tensile stress relaxation shall be defined as well. The following table summarizes the failure surface, the shear retention and stress relaxation factors for the four beams:

Parameter	B1	F1	S4	
			OC	SFRC OL/UL
$\beta_{t\,(OPEN)}$	0.3	0.15	0.3	0.1
$\beta_{t\,(CLOSE)}$	0.8	0.3	0.8	0.2
f_t	2.52	4.16	2.52	3.44
f_c	25.2	26	25.2	-1
f_{cb}	0	0	0	0
f_{amb}	0	0	0	0

Parameter	B1	F1	S4	
			OC	SFRC OL/UL
f_1	0	0	0	0
f_2	0	0	0	0
T_c	0.6	0.6	0.6	0.6

Table 3: Numerical Parameters used in the FE models

Since the failure surface can be calibrated using only uniaxial tensile and compressive strength, all three remaining parameters were set to zero.

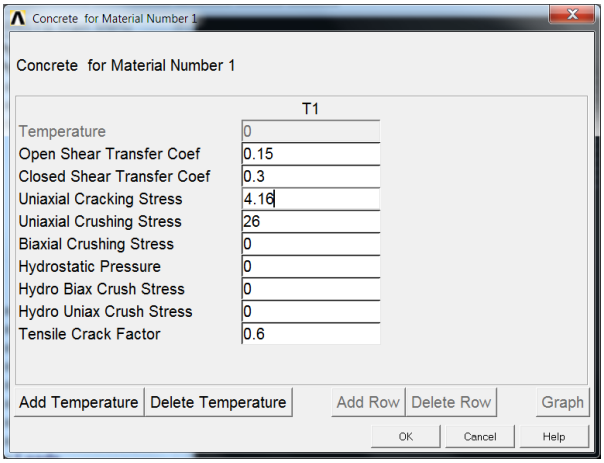

Figure 4-25: Material Parameters used for Beam F1-FEM

4.6 Reinforced Steel Modeling

Steel reinforcement is comparatively thin, and it is generally assumed to be capable of transmitting axial forces only. ANSYS presents element *LINK180* to model reinforcing steel, accurately. LINK180 is a spar that can be used in a variety of engineering applications. This element can be used to model trusses, sagging cables, links, springs, etc. This 3-D spar element is a uniaxial tension-compression element with three degrees of freedom at each node: translations in the nodal x, y, and z directions. As in a pin-jointed structure, no bending of the element is considered. Plasticity, creep, rotation, large deflection, and large strain capabilities are included. The element is not capable of carrying bending loads. The stress is assumed to be uniform over the entire element.

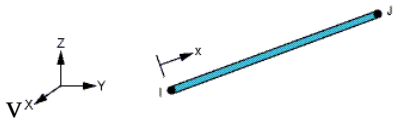

Figure 4-26: LINK180 Geometry

The element mass matrix described below is generated in the element coordinate system and then converted to the global coordinate system. The element stiffness matrix is:

$$\frac{\rho AL}{2}\begin{bmatrix}1 & 0 & 0 & 0 & 0 & 0\\ 0 & 1 & 0 & 0 & 0 & 0\\ 0 & 0 & 1 & 0 & 0 & 0\\ 0 & 0 & 0 & 1 & 0 & 0\\ 0 & 0 & 0 & 0 & 1 & 0\\ 0 & 0 & 0 & 0 & 0 & 1\end{bmatrix}$$

Where:

A = element cross-sectional area

L = element length

ρ = density

4.7 Steel Reinforcement Material Description

For steel reinforcement, a linear-elastic perfect-plastic material model was adopted. Since steel reinforcement is comparatively thin, it is generally assumed capable of transmitting axial force only; thus, a uniaxial stress-strain relationship is sufficient for general use. Due to all practical purposes, steel exhibits the same stress-strain curve in compression as in tension. Since steel reinforcement is used in concrete construction in the form of reinforcing bars or wire, it is not necessary to introduce the complexities of three-dimensional constitutive relations for steel.

For the models in hand, passion's ratio will be set to 0.3, modulus of elasticity will be set to 200 GPa, the yield strength for flexural reinforcement will be set to 420 MPa, while for secondary reinforcement and stirrups it will be set to 280 MPa. The tangent modulus for the flexural, secondary reinforcement and stirrups will be set to 2000 MPa.

4.8 Loading and Support Plates Modeling

Loading and support plates where modeled using element *SOLID185.* This element could be used for 3-D modeling of solid structures. It is defined by eight nodes having three degrees of freedom at each node: translations in the nodal x, y, and z directions. The element has plasticity, hyperelasticity, stress stiffening, creep, large deflection, and large strain capabilities. It also has mixed formulation capability for simulating deformations of nearly incompressible elastoplastic materials, and fully incompressible hyperelastic materials.

SOLID185 is available in two forms:

- Homogeneous Structural Solid.
- Layered Structural Solid.

SOLID185 Structural Solid is suitable for modeling general 3-D solid structures. It allows for prism and tetrahedral degenerations when used in irregular regions. Various element technologies such as B-bar, uniformly reduced integration, and enhanced strains are supported.

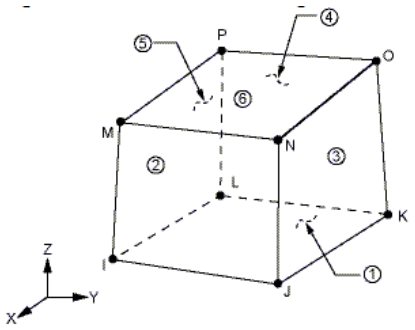

Figure 4-27: SOLID185 Homogeneous Structural Solid Geometry

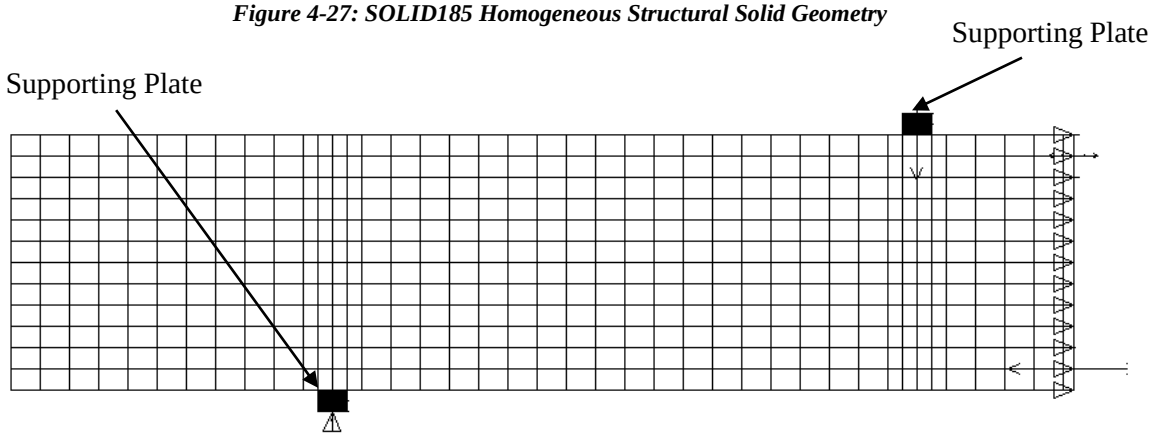

Figure 4-28: Loading and Support Plates

4.9 Model Structure

Establishing a FE model with proper mesh and proper constraint is a tedious work. Most of convergence problem arise from the use of improper mesh modeling, where element overlapping, constraint contradiction and watertight element problems could cause a significant divergence factor. To avoid the aforementioned problems, a handwritten code was developed to assure the integrity of the model. Nodes were created at certain positions to assure elements connectivity. Concrete and reinforcement elements were created and connected according to the reinforcement layout, to the same node to assure displacement compatibility.

Moreover, to ensure a full compatibility between the concrete and reinforcement elements, concrete nodes were merged with reinforcement nodes through the command "NUMMRG". This course of action would prevent any loose nodes and/or elements to float around the model, which would cause a numerical instability.

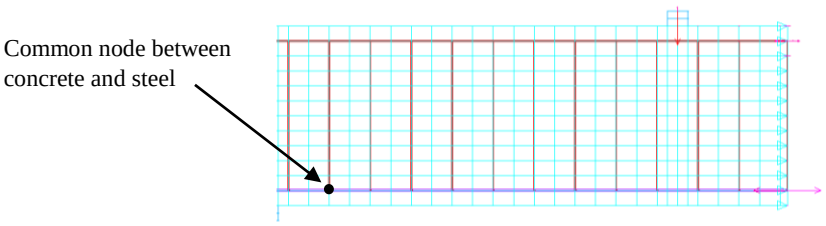

Figure 4-29: Concrete elements' nodes coincide with steel elements' nodes

Concrete elements were modeled using element "SOLID65". Tensile stress relaxation after cracking were included to help convergence and the stiffness multiplier for cracked tensile condition were set to 0.6. No real constants were used since smeared methodology of modeling reinforcement were excluded. Steel reinforcement were modeled using element "LINK180", with variable real constants depending on the cross-section of the reinforcement bar.

While concrete element contributes significantly to the nonlinearity of the model, a mesh convergence study were conducted on those elements, with a parametric variation in the x-direction dimension. Results indicated that an element with dimensions of 27.5mm×20mm×27.5mm in the x, y and z direction, respectively, would yield satisfactory results.

Reinforced steel elements were 55mm length for longitudinal reinforcement, and 27.5mm for transverse reinforcement. Concrete elements were densified in locations of contact with loading and supporting plates, this is to avoid any misinterpretation of stress values and, hence, prevent any distortion of concrete elements nearby those plates.

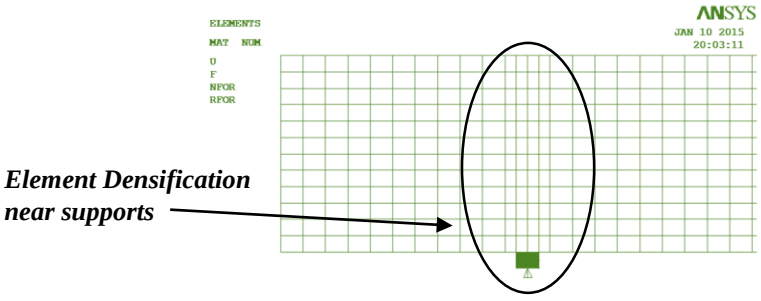

Figure 4-30: Concrete element densification near supporting plate

To save time and computational effort, and by taking advantage of symmetry along the midspan, only half of the beam were modeled. This requires applying additional boundary constrains, perpendicular to the axis of symmetry.

For the four beams, each model consisted of 20063 nodes, 3282 elements, 3 element types and 6 real constants. No coupling element, constraint equations or master DOF were used. For beam S4 overlay/underlay, in order to achieve a full monolithically behavior, a complete bonding is assumed between ordinary concrete and SFRC, thus, no contact element were used for the sake of simplicity.

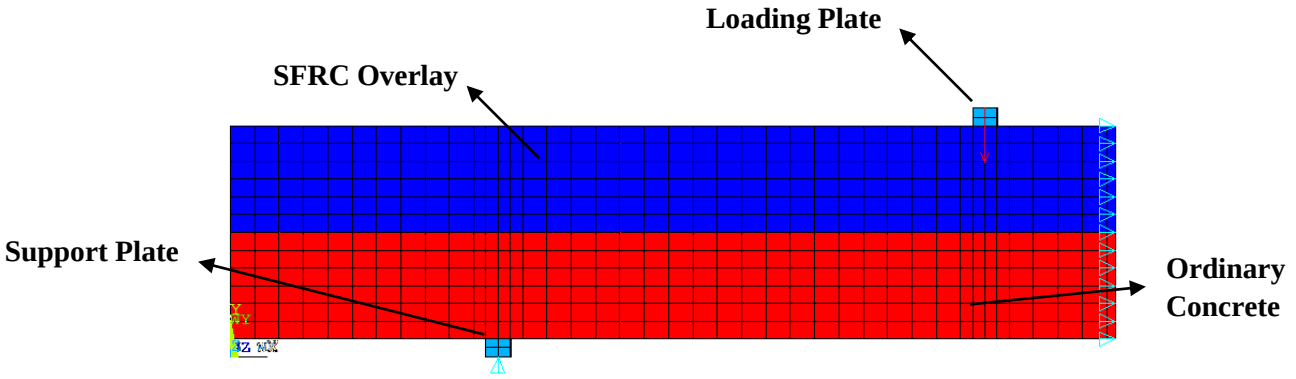

Figure 4-31: Beam S4 Overlay, Top Section (BLUE): SFRC, Bottom Section (RED): Ordinary Concrete, Loading plate and support plate (CYAN)

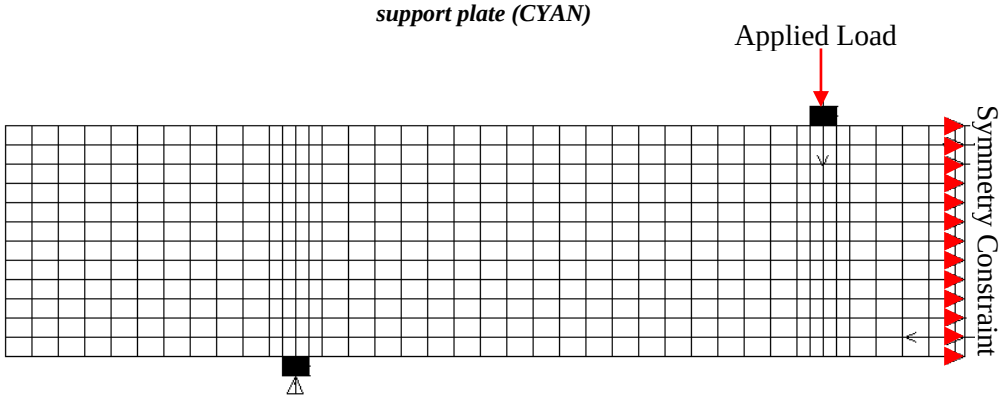

Figure 4-32: Constraints and Applied Load

4.10 Numerical Solution Parameters

Setting numerical solution parameters involves defining the analysis type and common analysis options for an analysis, as well as specifying load step options for it. A set of numerical solution controls must be identified to carry out a proper nonlinear analysis. Primarily, the analysis type was set to "Small Displacement Static". This means a linear and nonlinear analysis will be carried out to solve the models, in which large deformation effects are ignored. The load-applying

methodology in ANSYS is a function of time, where the load is considered as a fraction of a time substeps. It could be defined either by specifying the number of substeps or by defining a time incremental value. For the four beams, the second approach was considered, with time value at the end of load-step equal 1 second, a minimum and a maximum time step were 0.005 and 0.01, respectively, and a default time step equal to 0.01. Different values of minimum and maximum time step would allow automating the load value depending on convergence. Automated time stepping by placing an upper limit on the time step size especially for complicated models would enhance convergence process. The maximum number of equilibrium iteration was set to 100 iteration.

To solve the models, *ANSYS* has different equation solvers, i.e. SPARSE, PRE-CONDITION CG and ALGEBRAIC M-GRID. For the four beams, The "*Sparse Direct Solver*" was used. The sparse direct solver is based on a direct elimination of equations. Direct elimination requires the factorization of an initial very sparse linear system of equations into a lower triangular matrix followed by forward and backward substitution using this triangular system. The space required for the lower triangular matrix factors is typically much more than the initial assembled sparse matrix, hence the large disk or in-core memory requirements for direct methods.

The iterative process of Newton-Raphson method was used to solve the nonlinear equations of the model, along with the "*Line Search*" tool. To help the convergence process, the "*Line Search*" option was enabled. This convergence-enhancement tool multiplies the calculated displacement increment by a program-calculated scale factor (having a value between 0 and 1), whenever a stiffening response is detected. When an imposed displacement exists, a run cannot converge until at least one of the iterations has a line search value of one. ANSYS scales the entire ΔU vector, including the imposed displacement value; otherwise, a "small" displacement would occur everywhere except at the imposed DOF. Until one of the iterations has a line search value of one, ANSYS does not impose the full value of the displacement.

During the solving process, the program will continue to do equilibrium iterations until the convergence criteria are satisfied (or until the maximum number of equilibrium equations is reached). ANSYS' automatic solution control uses L2-norm of force (and moment) tolerance (TOLER) equal to 0.5%, a setting that is appropriate for most cases. In addition, an L2-norm check on displacement with tolerance value equal to 5% is also used in addition to the force norm check.

The check that the displacements are loosely set serves as a double-check on convergence, which was neglected for the four beams for the sake lowering the computational effort. For displacements, the program bases convergence checking on the change in deflections (Δu) between the current (i) and the previous (i-1) iterations: $\Delta u = u_i - (u_i - 1)$.

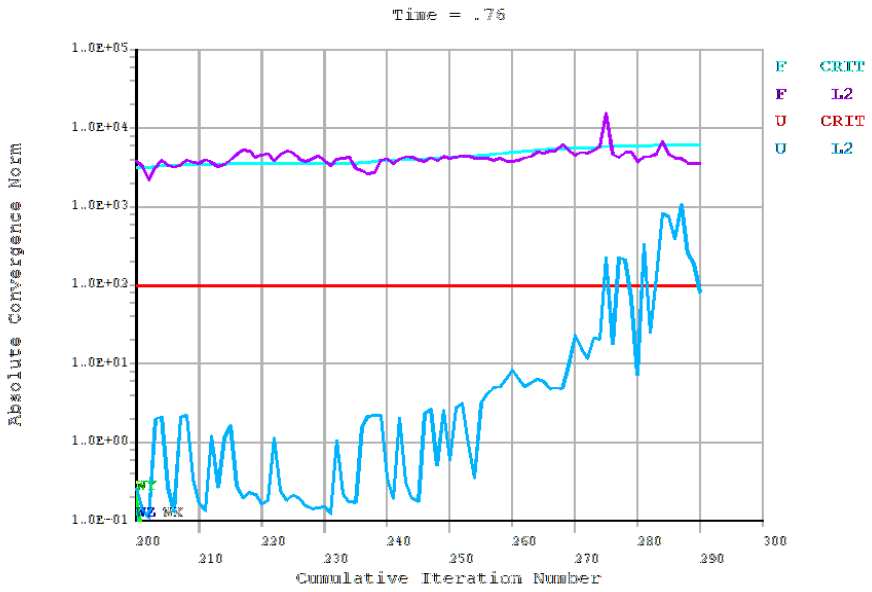

Figure 4-33: Convergence Tracking

CHAPTER 5
Discussion of FEA Results

As mentioned in the previous chapter, three numerical models have been investigated with the third one having two arrangements: overlay and underlay. All models had nonlinear material properties for concrete elements and linear-elastic perfect-plastic material properties for reinforcing steel. The first beam "*B1-FEM*" was considered as a control beam for comparison purposes, the second one "*F1-FEM*" is an exact replica of beam "*B1-FEM*", except it was modeled using SFRC material properties. The third beam "*S4-FEM*" has two arrangements: SFRC overlay and SFRC underlay. Geometrical and material information are as stated in chapter 4.

In the following sections, results regarding first crack load, yield load, plastic strain, failure load, failure deflection, crack pattern and load deflection curve will be presented.

5.1 BEAM "B1-FEM"

Beam "B1-FEM" is of a tension-control section designed according to ACI provisions. This beam is considered as a control beam for comparison purposes. It was modeling using ordinary concrete material properties. Shear failure of the beam was prevented using Ø8-mm stirrups every 55 mm in the shear span.

5.1.1 Load-Deflection Curve

As shown in **Figure 5-34** and **Figure 5-35** (d), a typical load deflection curve was obtained for the beam "B1-FEM". Linear and near linear behavior extended until the first crack where a sudden increase in deflection took place. Afterward, the linear behavior kept going until a load of 102.04 KN and a deflection of 3.9 mm. Beyond that, due to excessive crack proliferation, the beam experienced large increase of deflection under the same loading rate.

5.1.2 First Crack

As shown in **Figure 5-35** (a), first crack developed exactly at the midspan, a vertical flexural crack was initiated at load equal to 15.65 KN.

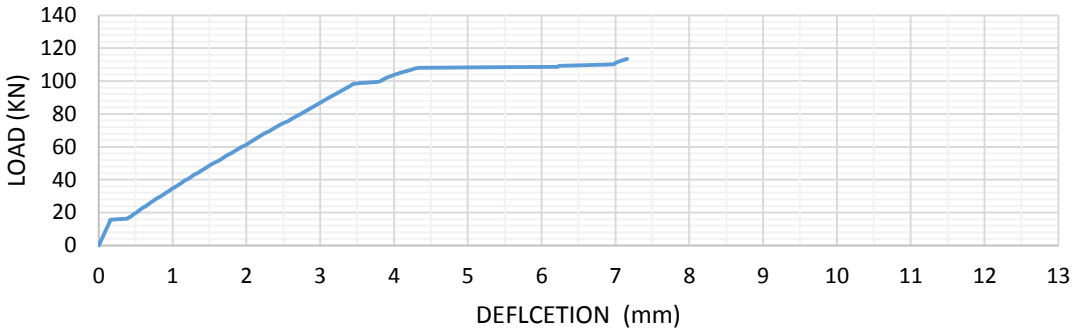

Figure 5-34: LOAD-DEFLECTION curve for Beam B1-FEM

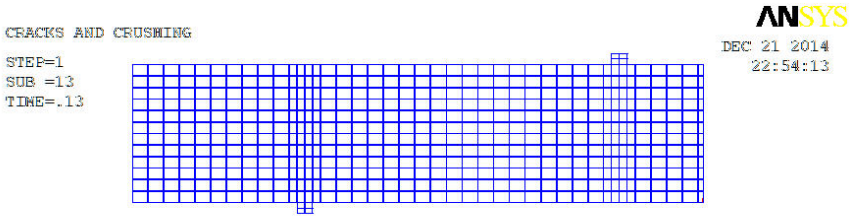

(a)

(b)

(c)

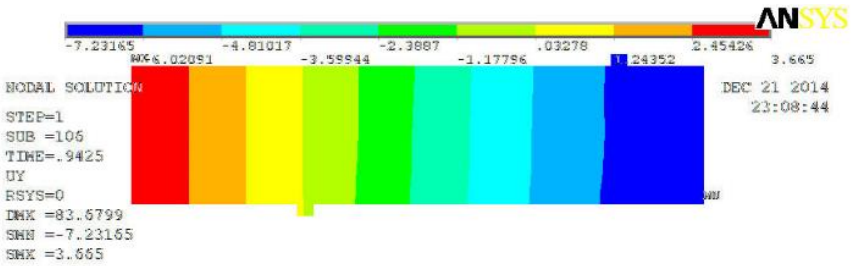

(d)

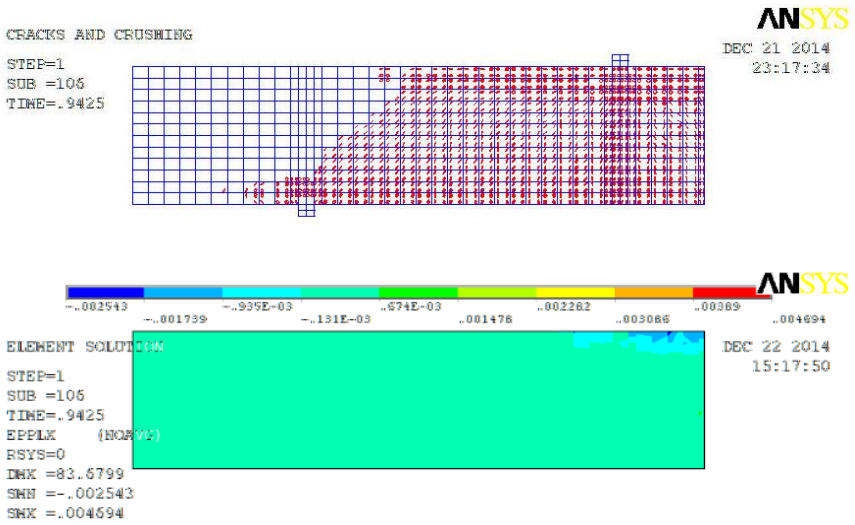

Figure 5-35: Beam "B1-FEM"-first crack (a), yielding (b), strain at failure (c), deflection at failure (d), crack at failure (e), strain at extreme compression fiber, concrete (f)

5.1.3 Yield Load and Strain at Failure

As shown in **Figure 5-35** (b) and (c), Results indicated that steel reinforcement would reach yield point at load equal to 103.24 KN. Yield of reinforcement occurs before complete failure of the beam. Plastic strain at complete failure equals to 0.007629 (mm/mm)

5.1.4 Failure Load, Failure Mode and Failure deflection

As shown in **Figure 5-35** (e), results indicated that beam would fail at load equal to 113.48 KN and a deflection equal to 7.23 cm. The beam failed in a typical ductile flexural manner. Flexural cracks developed and proliferated in the midspan, while diagonal cracks developed in the shear span. Failure of the beam occurred due to crushing of compression concrete in the midspan between two loading plates.

5.1.5 Strain on Extreme Compression Fiber at Failure

As shown in **Figure 5-35** (f), results indicated that the strain on extreme compression fiber at failure equals to 0.00254 mm/mm.

5.2 BEAM "F1-FEM"

Beam "F1-FEM" is an exact replica of beam "B1-FEM", except it was modeled using SFRC material properties. The SFRC was modeled using two techniques: 1. Smeared Model, 2. Discrete Model. This beam behaved in a ductile manner and reached its full flexural capacity.

Shear failure of the beam was prevented using Ø8-mm stirrups every 55 mm in the shear span. Flexural cracks were prevented from excessively proliferating in the compression zone at the midspan by steel fibers.

5.2.1 Load-Deflection Curve

As shown in **Figure 5-36** and **Figure 5-37** (d), a typical load deflection curve was obtained for the beam "F1-FEM". Linear behavior extended until first crack where a sudden increase in deflection took place. Afterward, the linear behavior kept going until a load of 114.71 KN and a deflection of 7.36 mm. Beyond that, due to crack excessive crack progression, the beam experienced large increase of deflection under the same loading rate.

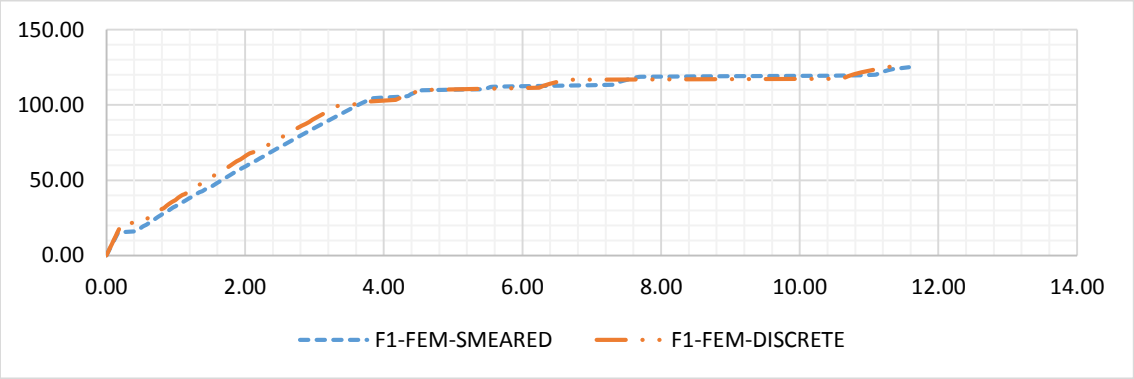

Figure 5-36: LOAD-DEFLECTION curve for Beam "F1-FEM", Both Smeared Model and Discrete

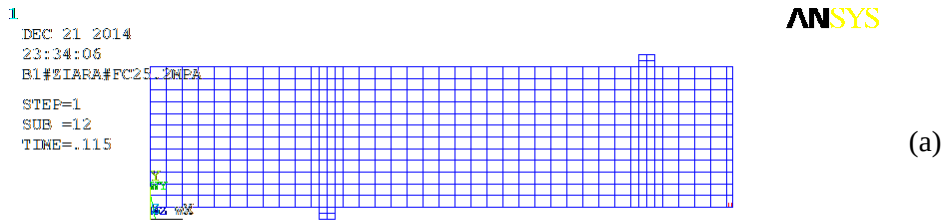

(a)

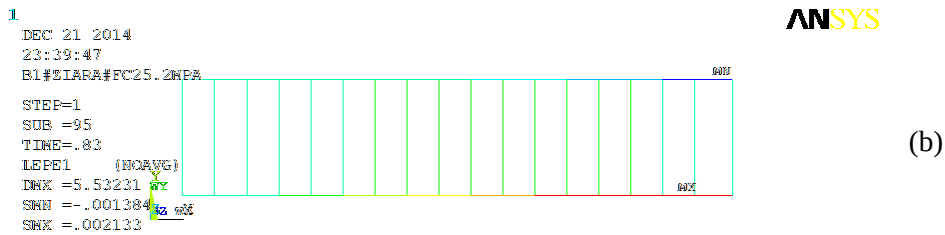

(b)

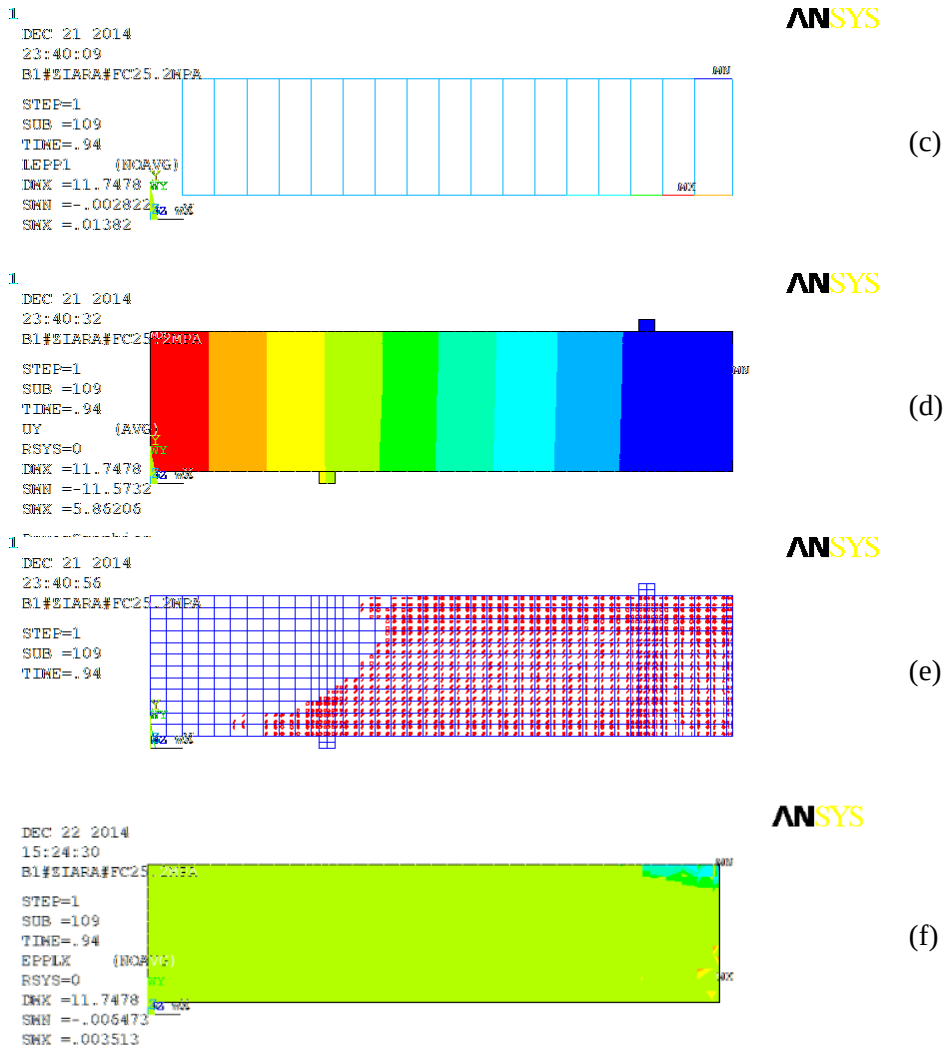

Figure 5-37: Beam "F1-FEM"-first crack (a), yielding (b), strain at failure (c), deflection at failure (d), crack at failure (e), strain at extreme compression fiber, concrete (f)

5.2.2 First Crack

As shown in **Figure 5-37** (a), first crack developed exactly at the midspan, a vertical flexural crack was initiated at load equal to 15.29 KN. It is worth mentioning that initial stress redistribution occurs as first crack was delayed due to existence of steel fibers to a load equal to 15.96 KN.

5.2.3 Yield Load and Strain at Failure

As shown in **Figure 5-37** (b) and (c), results indicated that steel reinforcement would reach yield point at load equal to 110.39 KN. Yield of reinforcement occurs before complete failure of the beam. Plastic strain at complete failure equals to 0.0132 (mm/mm).

5.2.4 Failure Load, Failure Mode and Failure deflection

As shown in **Figure 5-37** (e), results indicated that beam would fail at load equal to 125.02 KN and a deflection equal to 11.57 cm. The beam exhibited more ductile behavior than Beam "B1-FEM". Existence of steel fibers have enhanced both strength and ductility of the beam.

Flexural cracks developed and proliferated at midspan under increasing loads. Diagonal cracks were developed as well. Existence of steel fibers manage to minimize the splitting of compression concrete.

5.2.5 Strain on Extreme Compression Fiber at Failure

As shown in Figure **5-37** (f), results indicated that strain on extreme compression fiber at failure equals to 0.0054 mm/mm.

5.3 BEAM "S4-FEM-OL"

Beam "B4-FEM-OL" is a beam with half cross-section of ordinary concrete material properties and the other half with steel fiber reinforced concrete material properties. The SFRC section came on top as an overlay for strengthening purpose. The beam failed in a ductile manner and reached its full flexural capacity. Stirrups in underlay and overlay where connected together to simulate a welding situation. Shear failure was prevented using Ø8-mm stirrups in both ordinary concrete and SFRC overlay. Diagonal failure of the beam was prevented by stirrups in the overlay. Flexural cracks were prevented from excessively proliferating in the compression zone at the midspan by steel fibers. The beam exhibited a full interaction between SFRC overlay and ordinary concrete.

5.3.1 Load-Deflection Curve

As shown in **Figure 5-38** and **Figure 5-39** (d), a typical load deflection curve was obtained for the beam "S4-FEM-OL". Linear behavior extended until first crack where a sudden increase in deflection took place. Afterward, the linear behavior kept going until a load of 105.35 KN and a deflection of 3.77 mm. Beyond that, due to crack excessive crack progression, the beam experienced large increase of deflection under the same loading rate.

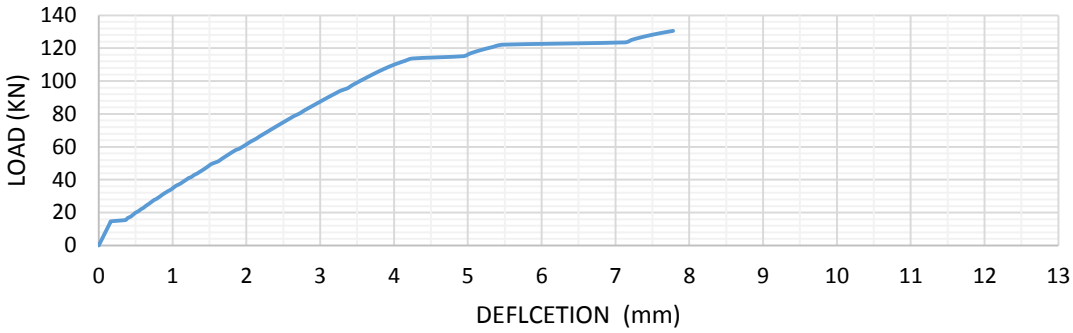

Figure 5-38: LOAD-DEFLECTION curve for Beam "S4-FEM-OL"

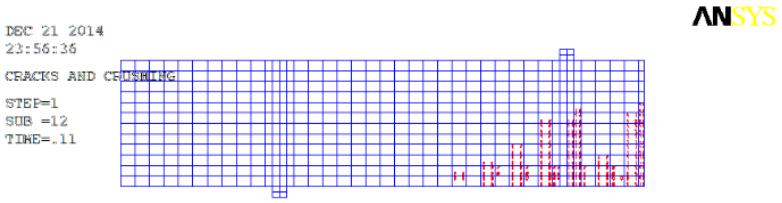

(a)

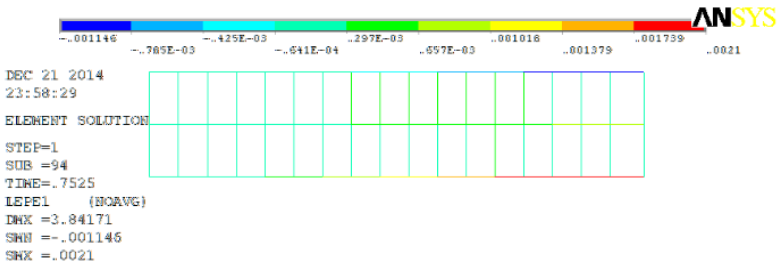

(b)

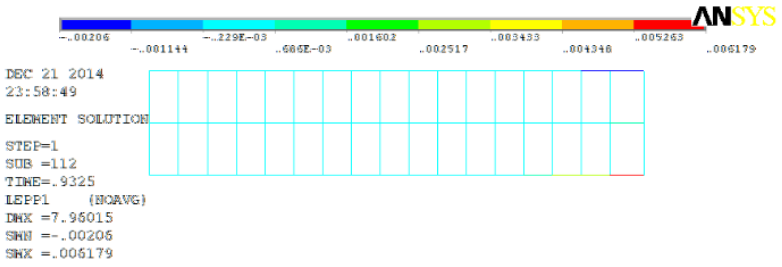

(c)

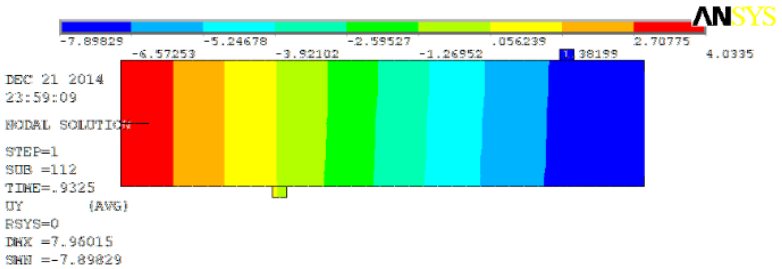

(d)

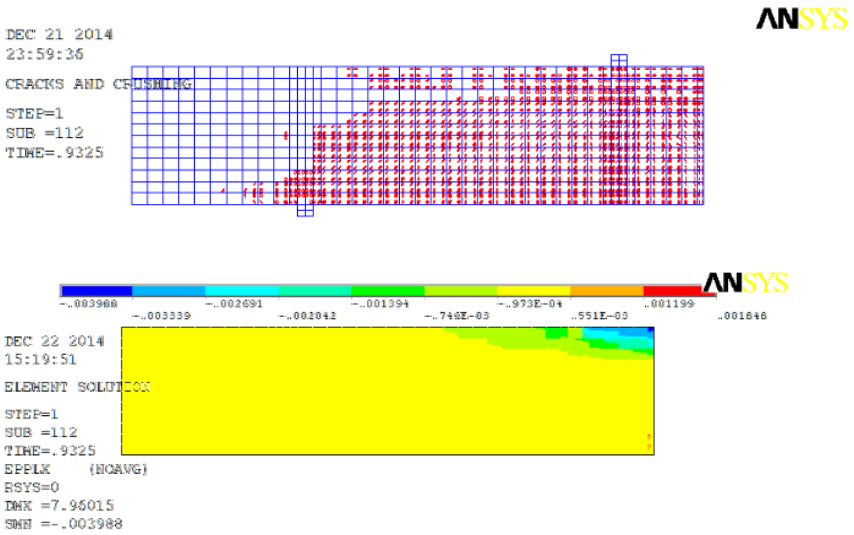

Figure 5-39: Beam "S4-FEM-OL"-first crack (a), yielding (b), strain at failure (c), deflection at failure (d), crack at failure (e), strain at extreme compression fiber, concrete (f)

5.3.2 First Crack

As shown in **Figure 5-39** (a), first crack developed exactly at the midspan, a vertical flexural crack was initiated at load equal to 15.05 KN. Diagonal cracks developed in the shear span around a load equal to 51.1 KN. Stirrups in the SFRC overlay managed to minimize the cracks proliferation to the compression zone.

5.3.3 Yield Load and Strain at Failure

As shown in **Figure 5-39** (b) and (c), results indicated that steel reinforcement would reach yield point at load equal to 105.35 KN. Yield of reinforcement occurs before complete failure of the beam. Plastic strain at complete failure equals to 0.00618 (mm/mm).

5.3.4 Failure Load, Failure Mode and Failure deflection

As shown in **Figure 5-39** (e), results indicated that the beam would fail at load equal to 130.55 KN and a deflection equal to 7.78 cm. flexural and diagonal cracks developed and proliferated in midspan and shear span. Stirrups in the overlay managed to minimize the cracks proliferation in the compression zone.

5.3.5 Strain on Extreme Compression Fiber at Failure

As shown in **Figure 5-39** (f), results indicated that strain on extreme compression fiber at failure equals to 0.0039 mm/mm

5.4 BEAM "S4-FEM-UL"

Beam "B4-FEM-UL" is a beam with half cross-section of ordinary concrete material properties and the other half with steel fiber reinforced concrete material properties. The SFRC section came as an underlay for strengthening purpose. This beam is a reverse one for "S4-FEM-UL". The SFRC underlay significantly improved the ductility behavior of the beam. The beam was able to reach its full flexural capacity. Stirrups in underlay and overlay where connected together to simulate a welding situation. Shear failure was prevented using Ø8-mm stirrups in both ordinary concrete and SFRC overlay. Diagonal failure of the beam was prevented by stirrups in the overlay. Flexural cracks were prevented from excessively proliferating in the compression zone at the midspan by steel fibers. The beam exhibited a full interaction between SFRC overlay and ordinary concrete.

5.4.1 Load-Deflection Curve

As shown in **Figure 5-40** and **Figure 5-41** (d), a typical load deflection curve was obtained for the beam "S4-FEM-UL". Linear behavior extended until first crack where a sudden increase in deflection took place. Afterward, the linear behavior kept going until a load of 117.60 KN and a deflection of 4.14 mm. Beyond that, due to crack excessive crack progression, the beam experienced excessive increase of deflection under the same loading rate.

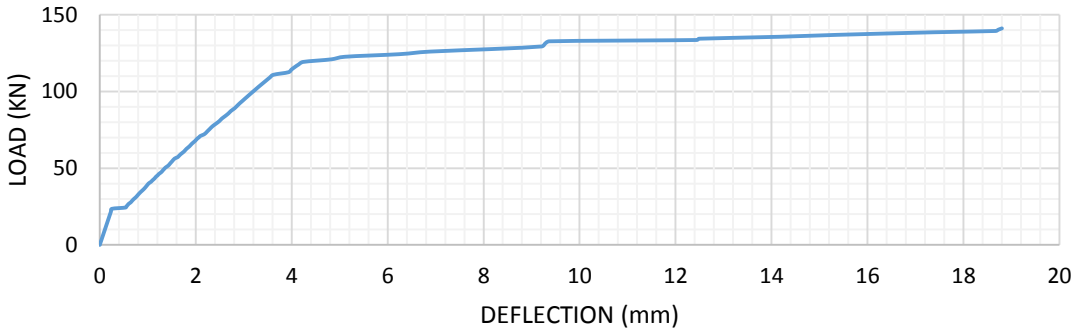

Figure 5-40: LOAD-DEFLECTION curve for Beam "S4-FEM-UL"

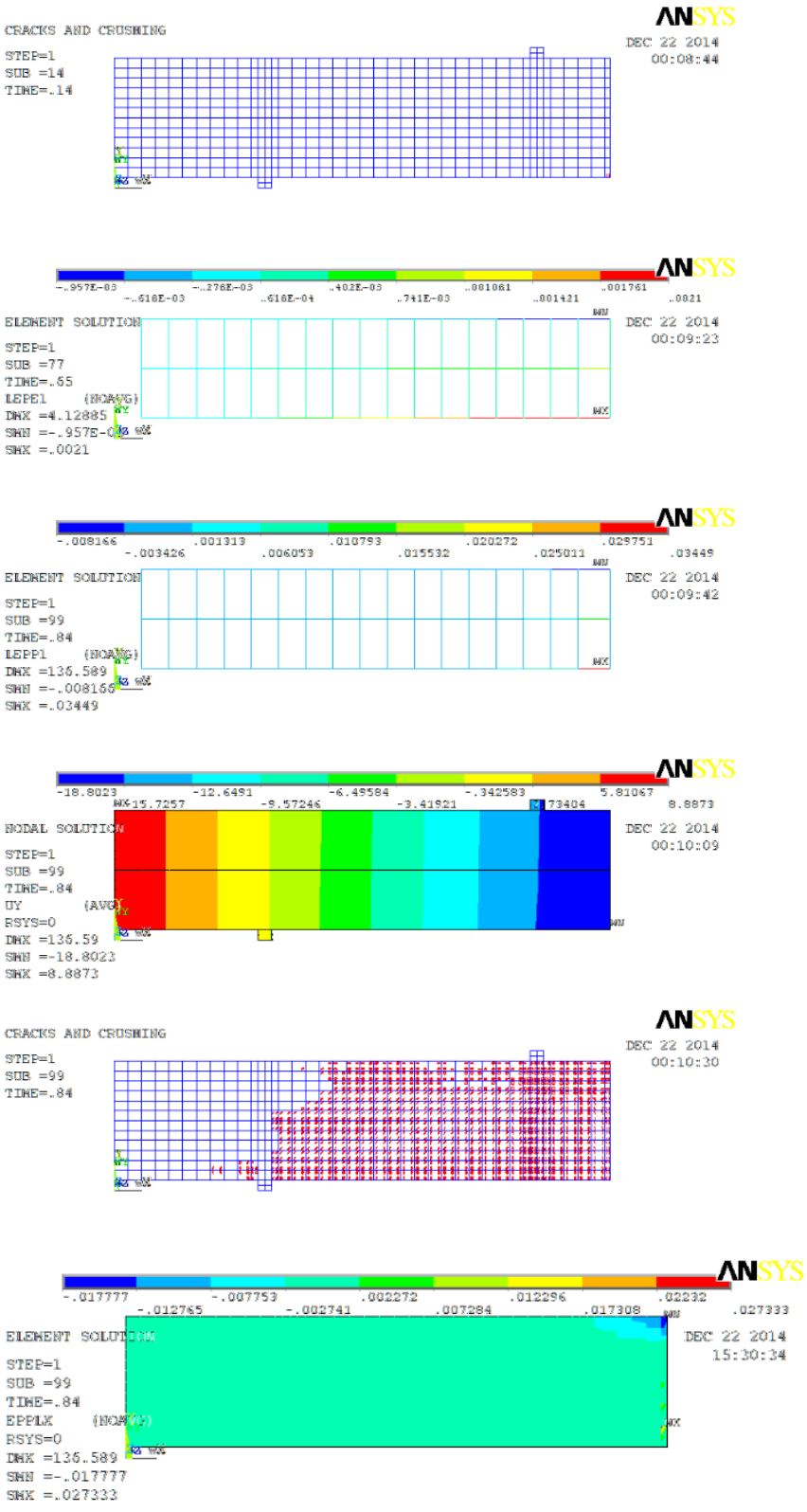

Figure 5-41: Beam "S4-FEM-UL"-first crack (a), yielding (b), strain at failure (c), deflection at failure (d), crack at failure (e), strain at extreme compression fiber, concrete (f)

5.4.2 First Crack

As shown in **Figure 5-41** (a), first crack developed exactly at the midspan, a vertical flexural crack was initiated at load equal to 23.52 KN. Diagonal cracks developed in the shear span around a load equal to 41.16 KN. Stirrups in the SFRC overlay managed to minimize the cracks proliferation to the compression zone.

5.4.3 Yield Load and Strain at Failure

As shown in **Figure 5-41** (b) and (c), results indicated that steel reinforcement would reach yield point at load equal to 109.20 KN. Yield of reinforcement occurs before complete failure of the beam. Plastic strain at complete failure equals to 0.0345 (mm/mm)

5.4.4 Failure Load, Failure Mode and Failure deflection

As shown in **Figure 5-41** (e), results indicated that the beam would fail at load equal to 141.12 KN and a deflection equal to 18.80 cm. Flexural and diagonal cracks developed and proliferated in midspan and shear span. Stirrups in the overlay managed to minimize the cracks proliferation in the compression zone.

5.4.5 Strain on Extreme Compression Fiber at Failure

As shown in **Figure 5-41** (f), results indicated that strain on extreme compression fiber at failure equals to 0.017 mm/mm

The following table summarizes the aforementioned results:

	B1-FEM	F1-FEM	S4-FEM-OL	S4-FEM-UL
First Crack Load (KN)	15.65	15.29	15.05	23.52
Yield Load (KN)	103.24	110.39	105.33	109.20
Strain At Failure (mm/mm)	0.0092	0.0132	0.0062	0.0345
Failure Load (KN)	113.48	125.02	130.55	141.12
Deflection (mm)	7.16	11.57	7.78	18.80
Failure Mode	Flexural	Flexural	Flexural	Flexural

Table 4: Summarization of Results for the Numerical Models

5.5 Comparison Of Results Against Experimental Data

The results of the numerical models were compared to results from experimental program of (Ziara, 2009) [10]. The experimental program consisted of nine beams with same material and geometrical properties. Only three beams were considered in this study. Beam "B1" was fabricated using traditional concrete and has the final dimensions of the strengthened beams. Beam "F1" is an identical to beam "B1", except it was fabricated using SFRC. Another set of beams with SFRC overlays were fabricated. The inter-laminar shear failure was resisted either chemically as in beams S1, S2 and S3, or mechanically as in beams S4 and S5. In this study, only beam S4 was considered.

Strengthened beams were made of two parts that have final cross-section of 150mm × 240 mm, which is equal to that used in the control beam "B1", and were provided with the same flexural reinforcement.

In general, the results of numerical models by ANSYS compares very well with those obtained from experimental program in terms of load carrying capacity, ductility and failure mode. Minor differences in load-deflection curves between numerical and experimental models can be attributed to the shortcomings in numerical material description, constitutive models and numerical instability in modeling the cracks.

5.3.1 Beams "B1-FEM" Vs. "B1"

Beams "B1-FEM" and "B1" were considered as control beams for numerical and experimental programs, respectively. Beam "B1-FEM" failed at a load equal 113.48 KN while beam "B1" failed at a load equal to 113.5 KN. The mid-span deflections at failure for beam "B1-FEM" was 7.16 mm, while mid-span deflection for beam "B1" was 7.58 mm. Both beams experienced a flexural failure in a typical ductile manner. The numerical values derivate from experimental values in terms of load failure and mid-span deflections by 0.017% and 5.54%, respectively.

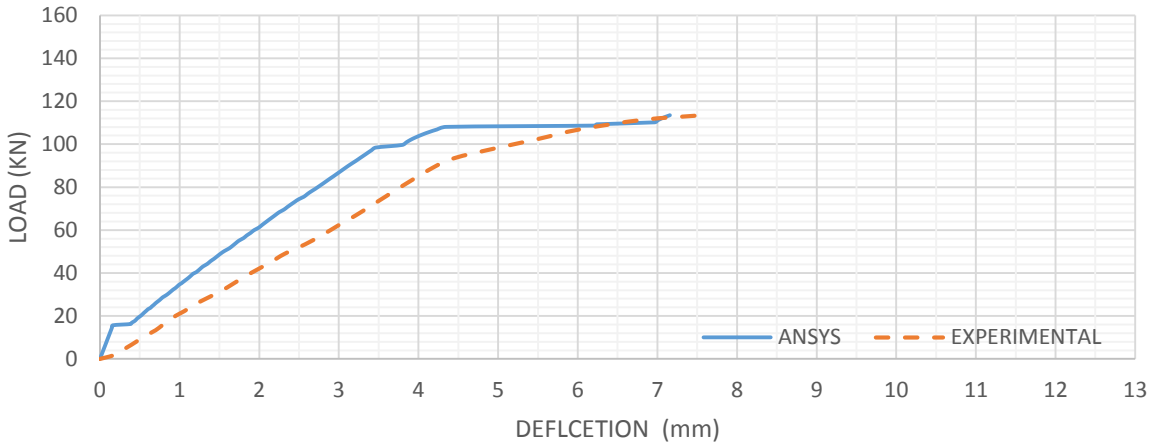

Figure 5-42: Beam "B1-FEM" (Numerical model) VS. Beam "B1" (Experimental model)

5.3.2 Beams “F1-FEM” Vs. “F1”

Beam “F1-FEM” failed at a load equal 125.02 KN while beam “F1” failed at a load equal to 126.80 KN. The mid-span deflections at failure for beam “F1-FEM” was 11.57 mm, while mid-span deflection for beam “F1” was 11.62 mm. Both beams experienced a flexural failure in a typical ductile manner. The numerical values derivate from experimental values in terms of load failure and mid-span deflections by 1.40% and 0.43%, respectively.

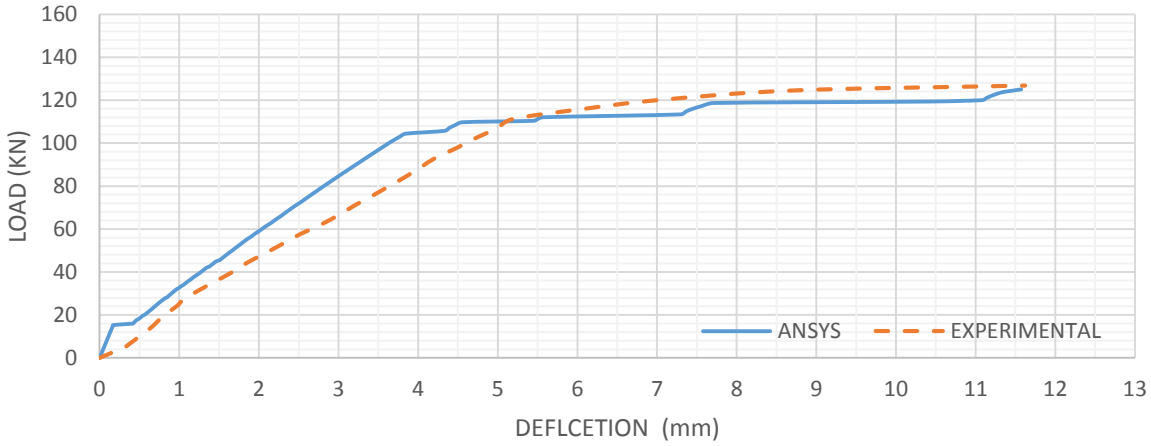

Figure 5-43: Beam "F1-FEM" (Numerical model) VS. Beam "F1" (Experimental model)

5.3.3 Beams “S4-FEM-OL” Vs. “S4”

Beam “S4-FEM-OL” failed at a load equal 130.55 KN while beam “S4” failed at a load equal to 133.50 KN. The mid-span deflections at failure for beam “S4-FEM-OL” was 7.78 mm,

while mid-span deflection for beam “S4” was 7.40 mm. Both beams experienced a flexural failure in a typical ductile manner. The numerical values derivate from experimental values in terms of load failure and mid-span deflections by 0.038% and 4.88%, respectively.

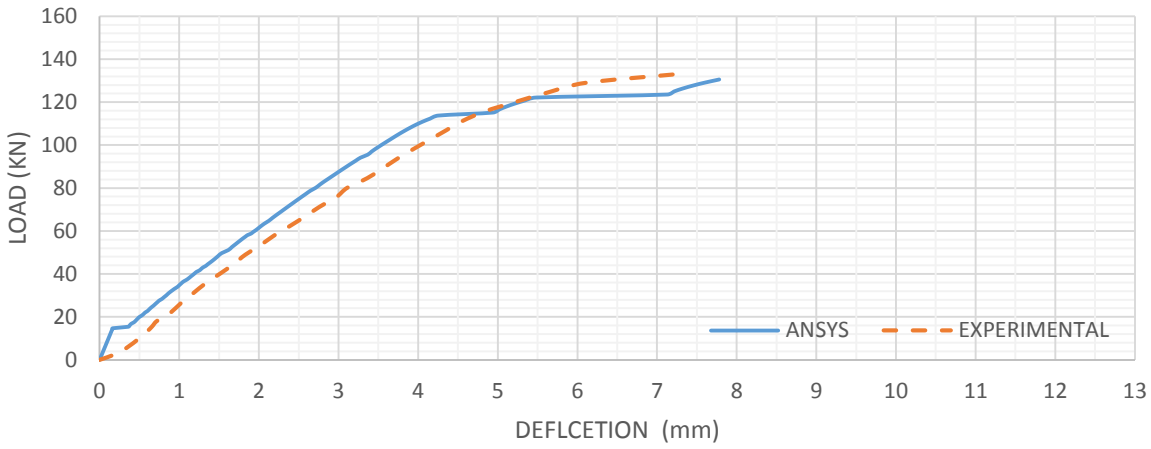

Figure 5-44: Beam "S4-FEM-OL" (Numerical model) VS. Beam "S4" (Experimental model)

Generally speaking, it is noticed that the FEA was able to capture the softening phenomena at first crack, major crack proliferation, yield point and just before complete failure, which is not clear in the experimental results. Furthermore, obtaining realistic results is highly dependent on the shear retention factors. Results would divert significantly when using improper SRF, hence the need for a toning process through the numerical analysis is vital. On the other hand, a change in passion’s ratio value did not affect the results significantly. Results that are more satisfactory would be obtained if experimental values of tensile strength, modulus of elasticity and passion’s ratio were incorporated into the numerical model, instead of using empirical formula to obtain those values.

Although crushing capabilities for SFRC overlays/underlays were turned off by assigning a value of -1 to compression strength parameter, both crack patterns and failure modes of numerical models compared very well to those of experimental models, this is mainly because failure of the models are controlled by proliferation of cracks into the concrete matrix rather than crushing of concrete.

5.6 Discussion

Beam "B1-FEM" was considered as a control beam where capacities of all other beams were compared to its capacity. For comparison purposes, the mid-span deflection were considered as a measurement of ductility. As expected, and since beam "B1-FEM" is a tension-control section designed according to ACI-318 provisions, a typical flexural failure has occurred.

For beam "F1-FEM", which was modeled using SFRC, the beam reached its full flexural capacity, which was equal to 125.02 KN, i.e. 1.1 of beam "B1-FEM". Due to presence of steel fibers, beam "F1-FEM" exhibit more ductile behavior than beam "B1-FEM". Presence of steel fibers is known to improve both ductility and tensile strength.

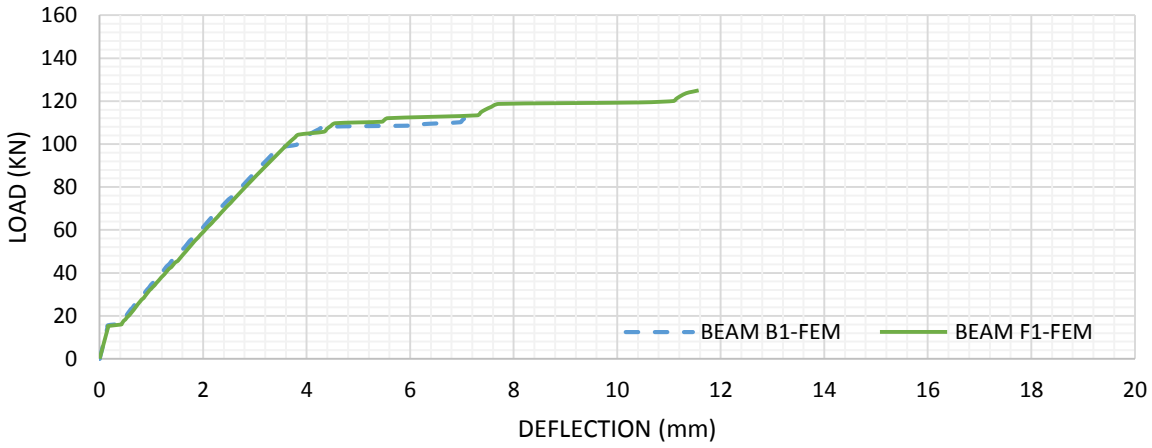

Figure 5-45: Beam "B1-FEM" VS. Beam "F1-FEM"

Beam "S4-FEM-OL" which is a strengthened beam with SFRC overlay containing stirrups in the shear span reached its full flexural capacity, which was equal to 130.55 KN, i.e. 1.15 of beam "B1-FEM". The increase of flexural capacity by 15% compared to control beam can be attributed to presence of steel fibers and prevention of inter-laminar shear failure by simulating a welding situation of stirrups in SFRC overlay to the existing stirrups in ordinary concrete part. However, ductility of the beam was similar to that of control beam. Absence of steel fiber from section under neutral axis where tensile stresses were formed led to significant proliferation of cracks and hence, beam behavior in terms of ductility was similar to the control beam modeled using ordinary concrete properties.

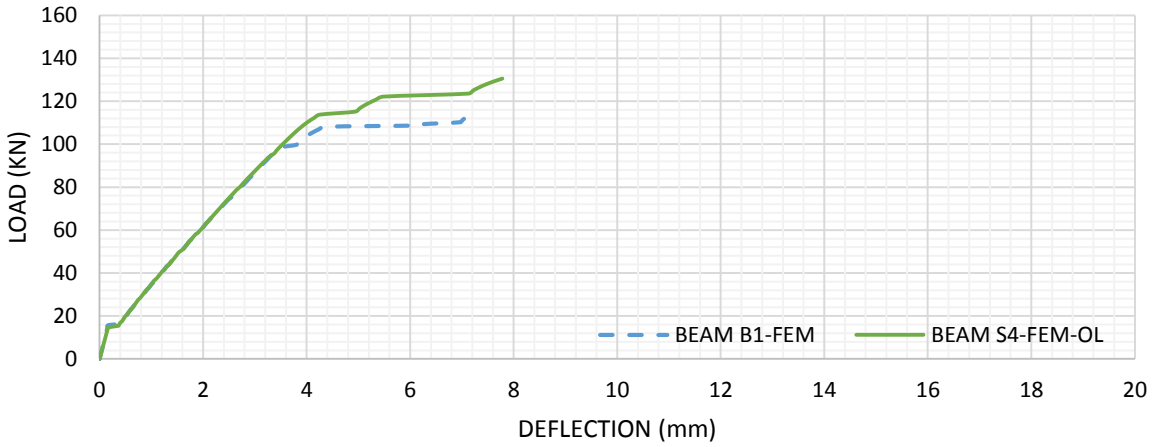

Figure 5-46: Beam "B1-FEM" VS. Beam "S4-FEM-OL"

Beam "S4-FEM-UL" which is a strengthened beam with SFRC underlay containing stirrups in shear span reached its full flexural capacity, which was equal to 141.12 KN, i.e. 1.24 of beam "B1-FEM". This beam experienced the highest flexural capacity of all four beams, which is a results prevention of inter-laminar shear failure by simulating a welding situation of stirrups in shear span of SFRC underlay to existing stirrups in ordinary concrete. Moreover, presence of steel fibers in concrete under neutral axis were tensile stresses were developed manage to delay first crack, prevent sudden cracks from developing and spreading under small amount of loads, and enhance stress redistribution between concrete and steel reinforcement.

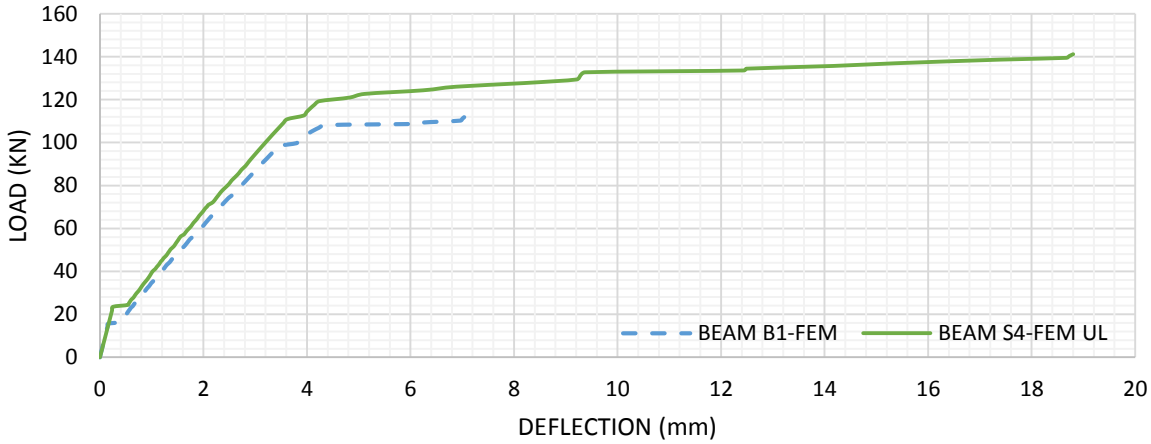

Figure 5-47: Beam "B1-FEM" VS. Beam "S4-FEM-UL"

Crack width for the aforementioned beams was not detectable. ANSYS is not equipped with discrete crack modeling technology, where crack width can be evaluated based on the separation

in the mesh. Smeared crack technology can predict both crack location and orientation but not crack width.

The sudden increase in the deflection at first crack for all of the beams is a reflection of stress redistribution phenomena, where concrete cannot withstand much longer tensile stress. In this case, steel reinforcement would resist those tensile stresses formed due to loading of beams. Presence of steel fibers can delay the stress redistribution as in beams "F1-FEM" to a certain load, where tensile stresses developed at that load cannot be resisted by steel fibers as well. The same thing goes for the "jumps" in deflection under a small rate of loading, during the entire loading process.

5.7 A parametric study

A parametric study was carried on beam "S4-FEM-OL". The influence of SFRC compressive strength and fraction volume on the overall behavior of the beam were examined. For the SFRC compressive strength, values of 31.5, 41.5 and 51.5 MPa were used. Those values represent an offset by 10 MPa from the experimental SFRC compressive strength. While values of 0.5%, 1% and 2% fraction volume were examined.

5.7.1 Effect of compressive strength on beam "S4-FEM-OL" behavior

The influence of compressive strength for the steel fiber-reinforced concrete were examined. Values of 31.5, 41.5 and 51.5 MPa were used. Results indicated a significant improvement in the load carrying capacity of the beam as well the overall ductility.

For a beam strengthened by SFRC overlay with a compressive strength of 31.5 MPa, the load carrying capacity at failure was 133.50 KN, i.e. 1.02 of beam "S4-FEM-OL" and almost the same as the experimental beam "S4". Due to the enhancement in compressive strength, the beam experienced a better ductile behavior, where deflection at failure was 10.55 mm, i.e. 1.35 of beam "S4-FEM-OL" and 1.42 of beam "S4".

For a beam strengthened by SFRC overlay with a compressive strength of 41.5 MPa, the load carrying capacity at failure was 145.95 KN, i.e. 1.11 of beam "S4-FEM-OL" and 1.09 of experimental beam "S4". Increasing the compressive strength affect the ductility of the beam significantly, where deflection at failure was 15.30 mm, i.e. 1.96 of beam "S4-FEM-OL" and 2.06 of beam "S4".

For a beam strengthened by SFRC overlay with a compressive strength of 51.5 MPa, the load carrying capacity at failure was 169.05 KN, i.e. 1.29 of beam "S4-FEM-OL" and 1.26 of experimental beam "S4". Out of the three compressive strength values, the best ductile behavior was reached, where deflection at failure was 22.94 mm, i.e. 2.94 of beam "S4-FEM-OL" and 3.1 of beam "S4".

The aforementioned results indicated a significant improvement in the beam behavior with the increase of compressive strength.

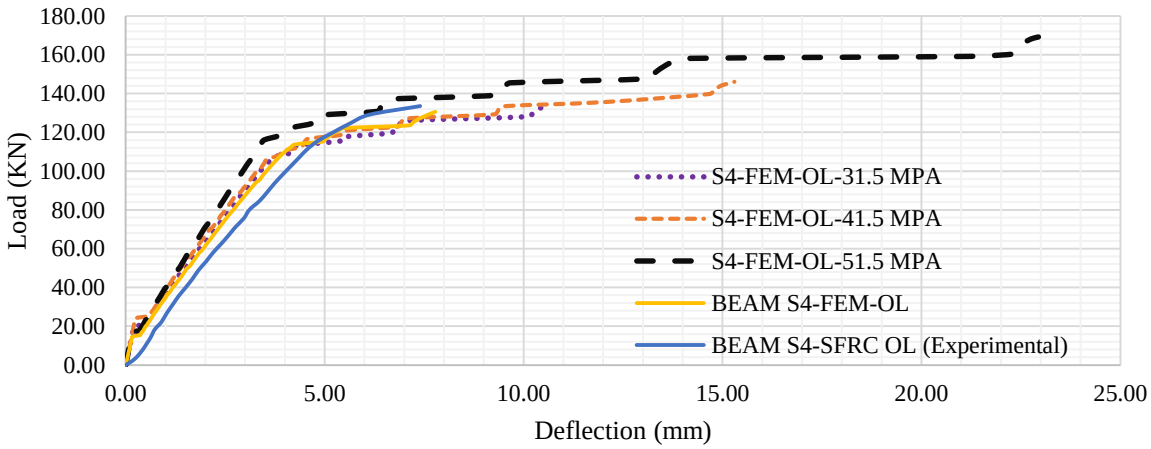

Figure 5-48: Effect of Compressive Strength on beam "S4-FEM-OL" behavior

5.7.2 Effect of Fraction volume on beam "S4-FEM-OL" behavior

Beam "S4-FEM-OL" was tested using 0.5%, 1%, and 2% fraction volumes. Results indicated an enhancement in the ductility of the beam at fraction volume of 2.0%. While the load carrying capacity maintain its original levels.

Increasing or decreasing in the fraction volume would not affect the overall behavior of the beam significantly. Mainly, because the SFRC overlay lie above the neutral axis where compressive stress are formed, while tensile stress to be resisted by the steel fibers are formed below the neutral axis.

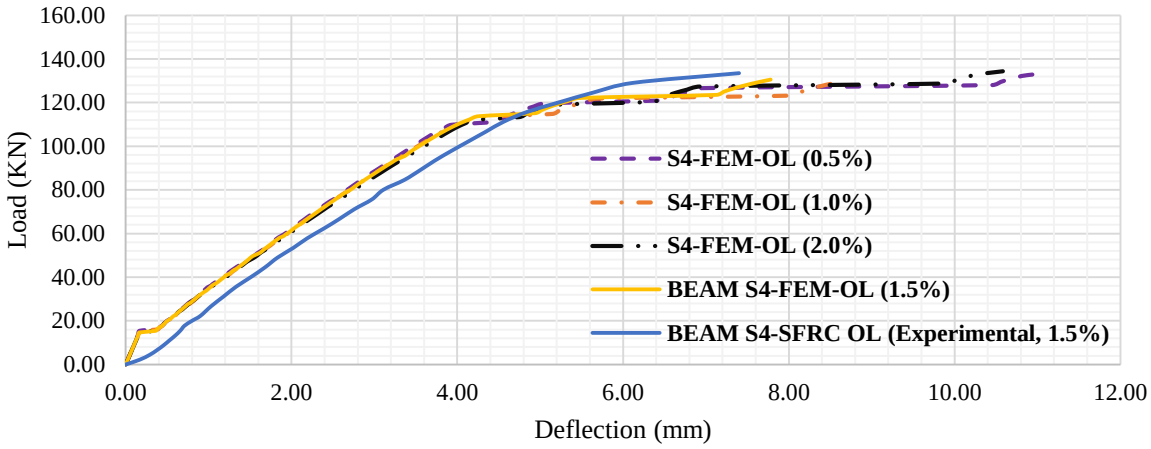

Figure 5-49: Effect of Volume Fraction on beam "S4-FEM-OL" behavior

CHAPTER 6
Summary and Conclusions

Experimental study of the behavior of reinforced concrete elements in the lab could be costly and time consuming because of fabrication consideration. This is where Finite Element Analysis (FEA) could be of a good help to study the RC structural elements behavior numerically and obtain satisfactory results compared to experimental results. ANSYS APDL v13.0 Finite element code is being tested throughout this thesis to study the behavior of RC beams strengthened with SFRC overlays and underlays. Four beams were tested, and results from numerical models were found to be in good agreement with those obtained from experimental models. The differences between results are within acceptable range.

With advancement in computer capabilities and progression in developing sophisticated constitutive models, modeling of traditional RC elements under different loading condition is an easy task nowadays. However, modeling of SFRC is still a wide field of research. A set of numerical parameters need to be tested in order to achieve a real-life response.

6.1 Conclusions

1. FEA could be used in predicting the behavior of RC beams strengthened with SFRC overlays or underlays.
2. FEA would save both time and cost involved in the actual experimental program.
3. Modeling of SFRC numerically can be done either by assuming homogenous material properties where steel fibers effect is to be "smeared" into the material properties and only one material description is to be used for SFRC modeling, or by assuming discrete material properties for steel fibers. In the latter case, two material description are needed to model SFRC. A force convergence tolerance of 0.005 would be suffice to obtain numerical results similar to experimental results. Using additional convergence tolerance, i.e. displacement with a value of 0.05, would refine the results and increase the load-deflection curve accuracy. However, more computational effort and time are required when using two convergence criteria.

4. Although compression part of Willam-Warnke failure surface could be disabled in structural elements expected to fail due to crack proliferation in order to get a numerical stable system, all beams were modeled with a full failure surface parameters. Modeling the steel fibers discretely did not affect the numerical stability of the beams when using the crushing capability of the code.

5. According to the numerical results, and when compared to the monolithical control beam, the load carrying capacity of RC beams strengthened with SFRC overlays can be improved by about 15%. For beams strengthened with SFRC underlays, the improvement goes far for about 24%. Ductile behavior and typical flexural failure were obtained for weld-bonded beams. Welding the stirrups in the shear span from overlay/underlay to the existing stirrups prevented the inter-laminar shear and diagonal tension failures, which results in a complete monolithical behavior until failure occurred.

6. Theoretically, using SFRC as an underlay shows a remarkable improvement in load carrying capacity and ductility. The ductility obtained by the SFRC underlay seems to control the overall ductility of the beam. Existence of steel fiber in the tension side of the beam helps improving the ductility and assure a better stress redistribution.

6.2 Recommendations

Based on the findings and results of the current work, the author recommends the following points to be addressed in any further studies:

1. More numerical studies are recommended to verify and demonstrate the capability of FEA in predicting the actual behavior of RC beams with different configuration.

2. Verify the numerical results of the SFRC underlay and the parametric study with experimental data.

3. Expand the scope of the numerical study to include RC beams bonded to SFRC overlays/underlays chemically. This includes using contact elements and fracture analysis.

4. Further examination to the effect of shear retention factors on behavior of SFRC, i.e. open and close, and develop a rational approach of choosing those factors.

5. Study the behavior of RC and SFRC beams simulated using a 3D plastic-damage concrete model and 3D stress-strain relationship.
6. Examine the failure load and failure patterns of RC and SFRC beams modeled, using different failure criteria, i.e. Drucker-Prager.

References

[1] G. Tiberti, F. Minelli and G. Plizzari, "Cracking behavior in reinforced concrete members with steel fibers- A comprehensive experimental study," *Cement and Concrete Research,* vol. 68, p. 24–34, 2015.

[2] X. Zhang, G. Ruiz and A. M. Abd Elazim, "Loading rate effect on crack velocities in steel fiber-reinforced concrete," *International Journal of Impact Engineering,* vol. 76, pp. 60-66, 2015.

[3] M. Paja¸k and T. Ponikiewski, "Flexural behavior of self-compacting concrete reinforced with different types of steel fibers," *Construction and Building Materials,* vol. 47, p. 397–408, 2013.

[4] X. Zhang, A. Abd Elazim, G. Ruiz and R. Yu, "Fracture behaviour of steel fibre-reinforced concrete at a wide range of loading rates," *International Journal of Impact Engineering,* vol. 71, pp. 89-96, 2014.

[5] T. Soetens and S. Matthys, "Different methods to model the post-cracking behaviour of hooked-end steel fibre reinforced concrete," *Construction and Building Materials,* vol. 73, p. 458–471, 2014.

[6] J. R. Deluce and F. J. Vecchio, "Cracking Behavior of Steel Fiber-Reinforced Concrete Members Containing Conventional Reinforcement," *ACI STRUCTURAL JOURNAL,* vol. 110, pp. 481-491, 2013.

[7] M. Özcan, A. Bayraktar, A. Sahin, T. Haktanir and T. Türker, "Experimental and finite element analysis on the steel fiber-reinforced concrete (SFRC) beams ultimate behavior," *Construction and Building Materials,* vol. 23, p. 1064–1077, 2009.

[8] M. A. Mansur and P. Paramasivam, "Steel fibre reinforced concrete beams in pure torsion," *The International Journal of Cement Composites and Lightweight Concrete,* vol. 4, no. 1, pp. 39-45, 1982.

[9] S. A. Al-Ta'an and J. R. Al-Feel, "Evaluation of Shear Strength of Fibre-Reinforced Concrete Beams," *Cement & Concrete Composites,* vol. 12, pp. 87-94, 1990.

[10] M. M. Ziara, "Behavior of Beams Strengthened with Steel Fiber RC Overlays," *Journal of Advanced Concrete Technology,* vol. 7, no. 1, pp. 111-121, 2009.

[11] J. G. MacGregor and J. K. Wight, Reinforced Concrete; Mechanics and Design, New Jersey: Pearson Education Inc,, 2009.

[12] Z. N. Taqieddin, Elasto-Plastic and Damage Modeling of Reinforced Concrete, Louisiana, USA: Louisiana State University, 2008.

[13] W.-F. Chen, Plasticity in Reinforced Concrete, New York: J. Ross Publishing, 2007.

[14] S. Shihada, Reinforced Concrete Design, Gaza: Manara Bookshop & Press, 2002.

[15] A. C. I. (ACI), "Building Code Requirements for Structural Concrete (ACI 318M-08) and Commentary," ACI, Michigan, 2008.

[16] E. Hognestad, N. W. Hanson and D. McHenry, "Concrete Stress distribution in Ultimate Strength Design," *ACI Journal,* vol. 52, no. 4, pp. 475-479, 1955.

[17] V. S. Gopalaratnam and S. P. Shah, "Softening response of plain concrete in direct tension," *International Journal of Rock Mechanics and Mining Sciences & Geomechanics Abstracts ,* vol. 23, no. 1, p. 310–323, 1986.

[18] H. Chen and R. Su, "Tension softening curves of plain concrete," *Construction and Building Materials,* vol. 44, no. 1, pp. 440-451, 2013.

[19] "The History of Fiber Reinforcement," Elasto Plastic Concrete, [Online]. Available: http://www.elastoplastic.com/index.php/the-history-of-fibre-reinforcement.

[20] M. Nataraja, N. Dhang and A. Gupta, "Stress-strain curves for Steel-Fiber Reinforced Concrete under compression," *Cement & Concrete Composites,* vol. 21, pp. 383-390, 1999.

[21] C. Juarez, P. Valdez, A. Duran and K. Sobolev, "The diagonal tension behavior of fiber reinforced concrete beams," *Cement & Concrete Composites,* vol. 29, p. 402–408, 2007.

[22] F. Altun, T. Haktanir and K. Ari, "Effects of Steel Fiber addition on mechanical properties of concrete and RC beams," *Construction and Building Materials,* vol. 21, pp. 654-661, 2007.

[23] K.-H. Tan, P. Paramasivam and K.-C. Tan, "Cracking Characteristics of Reinforced Steel Fiber Concrete Beams under Short- and Long-Term Loadings," *ADVANCED CEMENT BASED MATERIAL,* vol. 2, pp. 127-137, 1995.

[24] P. Song and S. Hwang, "Mechanical properties of high-strength steel fiber-reinforced concrete," *Construction and Building Materials,* vol. 18, p. 669–673, 2004.

[25] Y. Ding and W. Kusterle, "Compressive Stress-Strain Relationship of Steel Fiber-Reinforced Concrete at early age," *Cement and Concrete Research,* vol. 30, pp. 1573-1579, 2000.

[26] M. A. Mansur and P. Paramasivam, "Steel Fiber reinforced concrete beams in pure torsion," *The International Journal of Cement Composites and Lightweight Concrete,* vol. 4, no. 1, pp. 39-45, 1982.

[27] K. S. Kim, D. H. Lee, J. H. Hwang and D. A. Kuchma, "Shear behavior model for steel fiber-reinforced concrete members without transverse reinforcement," *Composites,* vol. 43, p. 2324–2334, 2012.

[28] J. A. Purkiss and P. J. Wilson, "Determination of the load-carrying capacity of steel fibre reinforced concrete beams," *Composite Structures,* vol. 38, no. 4, pp. 111-117, 1997.

[29] R. Cerioni and I. Iori, Three-Dimensional Numerical Modeling of Reinforced Concrete Behavior, Parma: University of Parma, 2006.

[30] D. Kachlakev and T. Miller, Finite Element Modeling of Reinforced Concrete Structures Strengthened With FRP Laminates, Washington: Federal Highway Administration, 2001.

[31] D. Darwin and D. A. Pecknold, "Analysis of Cyclic Loading of Plane R/C Structures," *Computers & Structures,* vol. 7, no. 1, pp. 137-147, 1977.

[32] M. D. Kotsovos and M. N. Pavlovic, Structural Concrete 'Finite-element analysis for limit-state design', Wiltshire: Thomas Telford, 1995.

[33] K. J. Willam and E. D. Warnke, "Constitutive Model for the Triaxial Behavior of Concrete," *International Association for Bridge and Structural Engineering,* vol. 19, p. 174. 1975, 1974.

[34] H. G. KWAK and F. C. FILIPPOU, "Finite Element Analysis of Reinforced Concrete Structures under Monotonic Loads," Structural Engineering, Mechanics and Materials, University of California, Berkeley, California, 1990.

[35] J. G. Rots and J. Blaauwendraad, *Crack Models for Concrete,* Delft: HERON, 1989.

Appendix: ANSYS APDL FEM code of beam *"B1-FEM"*

```
!! A Command-Line of Beam "B1-FEM"
!! ALL material description are included
!! Created by Mohammed H. Ashour


FINISH
/CLE
/NOPR
KEYW,PR_SET,1
KEYW,PR_STRUC,1
KEYW,PR_THERM,0
KEYW,PR_FLUID,0
KEYW,PR_ELMAG,0
KEYW,MAGNOD,0
KEYW,MAGEDG,0
KEYW,MAGHFE,0
KEYW,MAGELC,0
KEYW,PR_MULTI,0
KEYW,PR_CFD,0

/FILNAME,B1#ZIARA#FC25.2MPA,0
/CWD,'D:\ANSYS_SFRC_OVERLAYS\B1#ZIARA#FC25.2MPA'
/TITLE,B1#ZIARA#FC25.2MPA
/NOPR
KEYW,PR_SET,1

/PREP7
/UNITS,MPA
ET,1,SOLID65
ET,2,SOLID185
ET,3,LINK180

KEYOPT,1,1,1
KEYOPT,1,3,0
KEYOPT,1,5,1
KEYOPT,1,6,3
KEYOPT,1,7,1
KEYOPT,1,8,0
KEYOPT,2,2,0
KEYOPT,2,3,0
KEYOPT,2,6,0
KEYOPT,3,2,0

R,1,0,0,0,0,0,0,
R,3,50.26,0,
R,4,153.93,0,

MPTEMP,,,,,,,,
MPTEMP,1,0
!MPDE,EX,1
!MPDE,PRXY,1
MPDATA,EX,1,,26982
```

```
MPDATA,PRXY,1,,0.3
TBDE,MISO,1,,,
TB,MISO,1,1,14,0
TBTEMP,0
TBPT,,0.00028018,7.56
TBPT,,0.00038018,9.966
TBPT,,0.00048018,12.112
TBPT,,0.00058018,14.059
TBPT,,0.00068018,15.808
TBPT,,0.00078018,17.36
TBPT,,0.00088018,18.713
TBPT,,0.00098018,19.867
TBPT,,0.0010802,20.824
TBPT,,0.0011802,21.583
TBPT,,0.0012802,22.143
TBPT,,0.0013802,22.505
TBPT,,0.0014802,22.669
TBPT,,0.001513,22.68
TBDE,CONC,1,,,
TB,CONC,1,1,9,
TBTEMP,0
TBDATA,,0.3,0.8,2.52,25.2,0,0
TBDATA,,0,0,0.6,,,


MPTEMP,,,,,,,,
MPTEMP,1,0
!MPDE,EX,2
!MPDE,PRXY,2
MPDATA,EX,2,,2E+005
MPDATA,PRXY,2,,0.3
TBDE,BISO,2,,,
TB,BISO,2,1,2,
TBTEMP,0
TBDATA,,420,2000,,,,
MPTEMP,,,,,,,,
MPTEMP,1,0
!MPDE,EX,3
!MPDE,PRXY,3
MPDATA,EX,3,,2E+005
MPDATA,PRXY,3,,0.3
TBDE,BISO,3,,,
TB,BISO,3,1,2,
TBTEMP,0
TBDATA,,280,2000,,,,
MPTEMP,,,,,,,,
MPTEMP,1,0
!MPDE,EX,4
!MPDE,PRXY,4
MPDATA,EX,4,,2E+005
MPDATA,PRXY,4,,0.3
)/GOP    ! Resume printing after UNDO process

! -----------  MODELING ----------- !

/Prep7
```

```
! Concrete Nodes Arrangement
*DIM,XCOD,ARRAY,42,,,
XCOD(1)=0
XCOD(2)=27.5
XCOD(3)=55
XCOD(4)=82.5
XCOD(5)=110
XCOD(6)=137.5
XCOD(7)=165
XCOD(8)=192.5
XCOD(9)=220
XCOD(10)=247.5
XCOD(11)=275
XCOD(12)=288.75
XCOD(13)=302.5
XCOD(14)=316.25
XCOD(15)=330
XCOD(16)=357.5
XCOD(17)=385
XCOD(18)=412.5
XCOD(19)=440
XCOD(20)=467.5
XCOD(21)=495
XCOD(22)=522.5
XCOD(23)=550
XCOD(24)=577.5
XCOD(25)=605
XCOD(26)=632.5
XCOD(27)=660
XCOD(28)=687.5
XCOD(29)=715
XCOD(30)=742.5
XCOD(31)=770
XCOD(32)=797.5
XCOD(33)=825
XCOD(34)=838.75
XCOD(35)=852.5
XCOD(36)=866.25
XCOD(37)=880
XCOD(38)=907.5
XCOD(39)=935
XCOD(40)=962.5
XCOD(41)=990
XCOD(42)=1000


*DIM,YCOD,ARRAY,13,,,
YCOD(1)=20
YCOD(2)=40
YCOD(3)=60
YCOD(4)=80
YCOD(5)=100
YCOD(6)=120
YCOD(7)=140
```

```
YCOD(8)=160
YCOD(9)=180
YCOD(10)=200
YCOD(11)=220
YCOD(12)=240
YCOD(13)=260


*DIM,ZCOD,ARRAY,7,,,
ZCOD(1)=0
ZCOD(2)=20
ZCOD(3)=47.5
ZCOD(4)=75
ZCOD(5)=102.5
ZCOD(6)=130
ZCOD(7)=150



*SET,counterN,1                          !!!! initiating node sequance for nodes, start=1
*DO,counterX,1,42,1
*DO,counterY,1,13,1
*DO,counterZ,1,7,1

*SET,XCODIN,XCOD(counterX)
*SET,YCODIN,YCOD(counterY)
*SET,ZCODIN,ZCOD(counterZ)
n,counterN,XCODIN,YCODIN,ZCODIN
counterN=countern+1
*ENDDO
*ENDDO
*ENDDO


!! Support Plate Nodes Arrangement
*DIM,XSSCOD,ARRAY,3,,,
XSSCOD(1)=288.75
XSSCOD(2)=302.5
XSSCOD(3)=316.25


*DIM,YSSCOD,ARRAY,3,,,
YSSCOD(1)=0
YSSCOD(2)=10
YSSCOD(3)=20

*SET,counterN,10001                      !!!! initiating node sequance for nodes, start=10001
*DO,counterX,1,3,1
*DO,counterY,1,3,1
*DO,counterZ,1,7,1

*SET,XCODIN,XSSCOD(counterX)
*SET,YCODIN,YSSCOD(counterY)
*SET,ZCODIN,ZCOD(counterZ)
n,counterN,XCODIN,YCODIN,ZCODIN
counterN=countern+1
```

```
*ENDDO
*ENDDO
*ENDDO

!! Loading Plate Nodes Arrangement
*SET,counterN,20001                                    !!!! initiating node sequance for nodes, start=20001
*DIM,XSLCOD,ARRAY,3,,,
XSLCOD(1)=838.75
XSLCOD(2)=852.5
XSLCOD(3)=866.25



*DIM,YSLCOD,ARRAY,3,,,
YSLCOD(1)=260
YSLCOD(2)=270
YSLCOD(3)=280

*DO,counterX,1,3,1
*DO,counterY,1,3,1
*DO,counterZ,1,7,1

*SET,XCODIN,XSLCOD(counterX)
*SET,YCODIN,YSLCOD(counterY)
*SET,ZCODIN,ZCOD(counterZ)
n,counterN,XCODIN,YCODIN,ZCODIN
counterN=countern+1
*ENDDO
*ENDDO
*ENDDO

! ----------- ELEMENT GENERATION ----------- !
! CONCRETE ELEMENT GENERATION
TYPE,1
MAT,1
REAL,1
*SET,countNZ,7
*SET,countNY,13
*SET,countNX,42
*SET,NNUM,1
*SET,SCND,NNUM+countNZ*countNY


*DO,countELX,1,countNX-1,1
*DO,CountELY,1,countNY-1,1
*DO,CountELZ,1,countNZ-1,1
E,NNUM,NNUM+1,NNUM+1+CountNZ,countNZ+NNUM,SCND,SCND+1,SCND+1+countNZ,SCND+countNZ
NNUM=NNUM+1
SCND=SCND+1
*ENDDO
NNUM=NNUM+1
SCND=SCND+1
*ENDDO
NNUM=NNUM+countNZ
SCND=SCND+countNZ
```

```
*ENDDO

! SUPPORT PLATE ELEMENT GENERATION
TYPE,2
MAT,4
REAL,2
*SET,countNZ,7
*SET,countNY,3
*SET,countNX,3
*SET,NNUM,10001
*SET,SCND,NNUM+countNZ*countNY


*DO,countELX,1,countNX-1,1
*DO,CountELY,1,countNY-1,1
*DO,CountELZ,1,countNZ-1,1
E,NNUM,NNUM+1,NNUM+1+CountNZ,countNZ+NNUM,SCND,SCND+1,SCND+1+countNZ,SCND+countNZ
NNUM=NNUM+1
SCND=SCND+1
*ENDDO
NNUM=NNUM+1
SCND=SCND+1
*ENDDO
NNUM=NNUM+countNZ
SCND=SCND+countNZ
*ENDDO

! LOADING PLATE ELEMENT GENERATION
TYPE,2
MAT,4
REAL,2
*SET,countNZ,7
*SET,countNY,3
*SET,countNX,3
*SET,NNUM,20001
*SET,SCND,NNUM+countNZ*countNY

*DO,countELX,1,countNX-1,1
*DO,CountELY,1,countNY-1,1
*DO,CountELZ,1,countNZ-1,1
E,NNUM,NNUM+1,NNUM+1+CountNZ,countNZ+NNUM,SCND,SCND+1,SCND+1+countNZ,SCND+countNZ
NNUM=NNUM+1
SCND=SCND+1
*ENDDO
NNUM=NNUM+1
SCND=SCND+1
*ENDDO
NNUM=NNUM+countNZ
SCND=SCND+countNZ
*ENDDO

! STEEL REINFORCEMENT ELEMENT GENERATION
! KEYPOINTS GENERATION
*SET,KP,30001
*SET,KPXCOD,55
*DO,KPCounter,1,17,1
```

```
n,KP,KPXCOD,40,20
n,KP+1,KPXCOD,40,75
n,KP+2,KPXCOD,40,130
n,KP+3,KPXCOD,240,20
n,KP+4,KPXCOD,240,75
n,KP+5,KPXCOD,240,130

KPXCOD=KPXCOD+55
KP=KP+6
*ENDDO
!! FAR NODE GENERATION
n,KP,1000,40,20
n,KP+1,1000,40,75
n,KP+2,1000,40,130
n,KP+3,1000,240,20
n,KP+4,1000,240,75
n,KP+5,1000,240,130

! STIRRUPS ELEMENT GENERATION
TYPE,3 !! LINK180
MAT, 3 !! Stirrups
REAL,3 !! Stirrups

*SET,P1,30001
*DO,STRPCounter,1,18,1
E,P1,P1+1        - BOTTOM HORIZONTAL
E,P1+1,P1+2      - BOTTOM HORIZONTAL
E,P1+3,P1+4      - UPPER HORIZONTAL
E,P1+4,P1+5      - UPPER HORIZONTAL
E,P1,P1+3        - VERTICAL
E,P1+2,P1+5      - VERTICAL
P1=P1+6
*ENDDO

! BOTTOM REINROCEMENT
TYPE,3 !! LINK180
MAT, 2 !! BOTTOM REINFORCEMENT
REAL,4 !! Stirrups
*SET,P1,30001
*DO,BTMSCounter,1,17,1
E,P1,P1+6
E,P1+2,P1+8
P1=P1+6
*ENDDO

!! ------- UPPER REINROCEMENT
TYPE,3 !! LINK180
MAT, 3 !! BOTTOM REINFORCEMENT
REAL,3 !! Stirrups
*SET,P1,30004
*DO,BTMSCounter,1,17,1
E,P1,P1+6
E,P1+2,P1+8
P1=P1+6
*ENDDO
```

```
NPLOT
NUMMRG,NODE, , , ,LOW
FLST,2,9,1,ORDE,2
FITEM,2,10028
FITEM,2,-10036


/PREP7
FLST,2,7,1,ORDE,2
FITEM,2,10022
FITEM,2,-10028
FLST,2,7,1,ORDE,2
FITEM,2,10022
FITEM,2,-10028
!*
/GO
D,P51X, , , , , ,UY, , , , ,
FLST,2,91,1,ORDE,2
FITEM,2,3732
FITEM,2,-3822
!*
/GO
D,P51X, , , , , ,UX, , , , ,
FLST,2,7,1,ORDE,2
FITEM,2,20036
FITEM,2,-20042
!*
/GO
F,P51X,FY,-8600
)/GOP    ! Resume printing after UNDO process


/SOL
ANTYPE,0
CNVTOL,F, ,0.05,2,-1,
DELTIM,0.01,0.005,0.01
TIME,1
CUTCONTROL,CRPLIMITexp,.1,0
CUTCONTROL,DSPLIMIT,10e6
CUTCONTROL,PLSLIMIT,.15
NCNV,2,0,0,0,0
AUTOTS,1
NEQIT,100
OUTRES,ALL,1
NROPT,FULL
LNSRCH,ON
NLGEOM,0
EQSLV,SPAR
```